APPLICATIONS OF NON-LINEAR METHODS IN ASTRONOMY

P.C.H. MARTENS

The Astronomical Institute at Utrecht, Space Research Laboratory,
Beneluxlaan 21, 3527 HS Utrecht, The Netherlands

NORTH-HOLLAND–AMSTERDAM

PHYSICS REPORTS (Review Section of Physics Letters) 115, No. 6 (1984) 315–378. North Holland, Amsterdam

APPLICATIONS OF NON-LINEAR METHODS IN ASTRONOMY

P.C.H. MARTENS[1]

The Astronomical Institute at Utrecht, Space Research Laboratory, Beneluxlaan 21, 3527 HS Utrecht, the Netherlands

Received May 1984

Contents:

Abstract:

In this review I discuss *catastrophes*, *bifurcations* and *strange attractors* in a non-mathematical manner by giving very simple examples that still contain the essence of the phenomenon. The salient results of the applications of these non-linear methods in *astrophysics* are reviewed and include such diverse phenomena as solar flares and loop brightenings (catastrophes), formation of binaries and cyclic stellar winds (bifurcations) and the solar cycle and galactic dynamics (strange attractors). Emphasis is laid on the unifying concept of *non-linearity* in (simple) differential equations that can be the framework for understanding and predicting such diverse phenomena as mentioned above. Finally there is a discussion on the concept of *intrinsic unpredictability* (as a result of non-linearity), the limit it sets to the use of numerical models and the way it contradicts our intuitive notions on deterministic systems.

[1] From October 1, 1984: Laboratory for Astronomy and Solar Physics, Code 682, NASA, Goddard Space Flight Center, Greenbelt, MD 20771, U.S.A.

Single orders for this issue

PHYSICS REPORTS (Review Section of Physics Letters) 115, No. 6 (1984) 315–378.

Copies of this issue may be obtained at the price given below. All orders should be sent directly to the Publisher. Orders must be accompanied by check.

Single issue price Dfl. 39.00, postage included.

1. Introduction

This review will be concerned with non-linear differential equations. Many problems in physics and related sciences are described by differential equations and most of them are non-linear. There are no general methods for solving these equations and although great ingenuity has been deployed in the treatment of many types of non-linear problems most non-linear equations remain unresolved. Also, in those non-linear equations that *have* been solved analytically there is a fundamental bias in the types of solutions that are found, simply because one can only solve analytically those problems that *can* be solved. Most non-linear problems are essentially irreducable to integral form and the necessary numerical solutions of these types of problems exhibit features that have no counterparts in integrable non-linear equations.

In the last few years considerable progress has been made with non-linearities. On one hand analytical methods have been developed that can extract important information from non-linear equations without actually solving them. On the other hand, the use of computers has led to important progress in understanding the nature of the solutions of equations that cannot be handled by any analytical method. Progress has been greatest in the understanding of turbulence in fluid mechanics and non-integrable Hamiltonian systems in statistical mechanics. The use of these methods is now spreading into the more peripheral natural sciences. However, it must be noted that actually some of these peripheral sciences have initiated the recent developments in fluid mechanics and statistical mechanics. Ecology has revived the interest in difference equations and mappings (section 4.2), the first strange attractor comes from the field of meteorology (section 4.3) and the Hénon–Heiles system of equations (section 4.4) from dynamical astronomy has become the standard model for the onset of stochasticity in statistical mechanics.

In this review I will discuss some of the important developments in non-linear differential equations and I will emphasize the application of the various methods in astronomy. The methods of dealing with non-linearities are presented in the form of simple examples that can be checked easily but that still contain the essence of the formalism. Thus abstract general theories and lengthy and laborious calculations are avoided. From the examples one might get the impression that non-linear problems are easily solved. This is not so: computations in real physical problems are often very complicated. This is usually a great drawback in studying the underlying methods. Therefore I shall start in a very simple manner, although it may seem oversimplified to experts.

An important phase in the solution of a problem that is ignored in this paper is the model building. The reason for this is that there are no general rules: each problem has its own pecularities justifying an individual approach. Model building is necessary because the general equations describing a problem are generally far too complicated to be solved directly, even by computer.

In non-linear model building those non-linear terms are retained in the simplified equations that describe the non-linearities that are thought to be relevant. Different types of non-linear models may be distinguished:

1. *The mathematical simulacrum.* A set of non-linear equations is used that is known to have solutions that exhibit phenomena that are similar to what is observed. The model equations may have nothing to do with the actual problem. The purpose of this kind of modelling is merely to show that non-linearities indeed may lead to solutions that behave as strangely as the observations. Examples are the Rössler equations (section 4.3), the solutions of which bear strong analogies with the results of experiments on turbulence.

2. *Ad hoc equations.* One starts with the governing equations and simplifies them using some

plausibility arguments about the effects that are going to dominate the solutions. This modelling is on somewhat firmer grounds than the previous one, but still there is no direct relation between the original and the model equations. Examples of this are the dynamo equations (section 4.5) and the equations for the plasma in coronal loops (section 3.4).

3. *Approximated equations.* The governing equations are reduced to a simpler form with the use of some – possibly severe – approximations. The difference with the ad hoc equations is that one can check from the results their consistency with the approximations. Consistent results are *valid* solutions of the governing equations, but the model probably does not describe all possible solutions.

In the following I shall deal with three main aspects of the solutions of non-linear equations. These are catastrophes (section 2), bifurcations (section 3), and strange attractors (section 4). Emphasis is laid upon their applications in astronomy. Solitons will not be discussed in this paper since there are already so many applications of soliton theory in astrophysics that this would require a review of its own.

2. Catastrophe theory

2.1. Theory

Catastrophe theory is not so much a theory as a conceptual framework. Many of its results are not new, but the way they are put together makes the conception a very transparent one, that is easily understood and applied in all sorts of fields, also outside that of the physical sciences. For some examples of these applications I refer to a book with selected papers by Zeeman [1], a popular paper by the same author [2] and a book by Poston and Stewart [3] with many physical examples. For the topological foundations of the theory I refer to a book by Thom [4], the inventor of catastrophe theory.

Catastrophe theory applies to those situations where gradually changing parameters lead to sudden changes in the variables. Depending upon the number of parameters and variables in the problem concerned a number of elementary catastrophes may occur. Here I will only be concerned with the simple 'cusp' catastrophe, for two changing parameters and one variable. In most astrophical examples this is then further reduced to a 'fold' catastrophe with only one parameter.

Consider a system described by the following differential equation

$$\dot{x} = bx - x^3 + p \tag{2.1.1}$$

where $\dot{x}$ is the derivative of x with respect to time. In this expression there are two parameters, of which one (b) will be kept constant, (the reason for introducing b will become apparent in section 3.1). The other parameter (p) is assumed to vary on a time scale that is larger than the typical time scale for x to reach its static equilibrium. The static equilibria of (2.1.1) are characterized by $\dot{x} = 0$ and the solution is given by

$$p = x_e^3 - bx_e\,. \tag{2.1.2}$$

The solution is displayed graphically in fig. 2.1 for $b > 0$. For $b < 0$ there is only one p for a given x_e; a situation that I shall not be concerned with in this section. By a simple graphical transformation fig. 2.2 is obtained, which depicts the static solution x_e as a function of the parameter p. Note that for certain values of p there are *multiple* solutions for x_e.

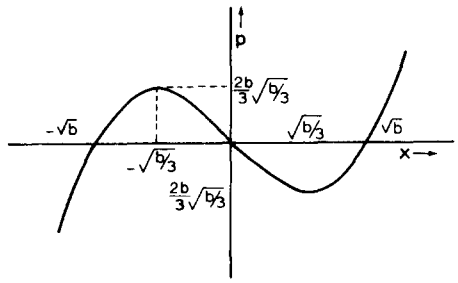

Fig. 2.1. The solution of eq. (2.1.2).

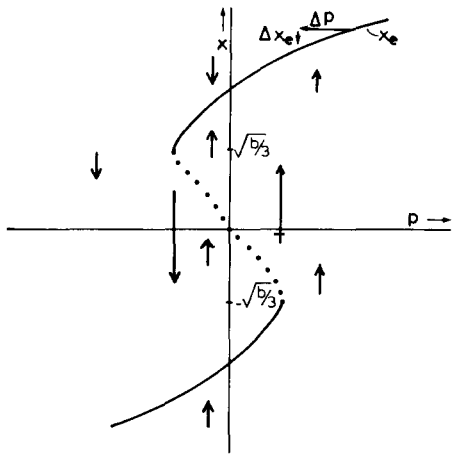

Fig. 2.2. The catastrophe picture of eq. (2.1.2).

The stability of the static solution may be investigated by the usual method of first order perturbations to the static solutions. The resulting *linear* differential equation for the perturbation $\varepsilon = x - x_e$ is

$$\dot{\varepsilon} = (b - 3x_e^2)\varepsilon \,. \tag{2.1.3}$$

Thus the solutions are stable for $|x_e| > \sqrt{b/3}$ and unstable for $|x_e| < \sqrt{b/3}$. The stability at $|x_e| = \sqrt{b/3}$ depends on higher order terms. The point can be proved to be unstable in this case. The unstable static equilibria are dotted in fig. 2.2. Now, for given values of b and p and a given initial value of x one may follow the evolution of x without explicitly solving eq. (2.1.1). At any given point the direction of the evolution, that is the sign of $\dot{x}$, can easily be calculated. This direction is indicated by the arrows in fig. 2.2. The equilibrium curve, defined by $\dot{x} = 0$ divides the regions with $\dot{x} < 0$ and $\dot{x} > 0$. It is also evident that there are no runaway solutions – i.e. solutions with $|x| \to \infty$ – because for large $|x|$ the non-linear term in (2.1.1) dominates.

After a certain time all solutions must converge to one of the two branches of stable static equilibria. Now, suppose that p changes – as a result of some process that is not incorporated in eq. (2.1.1) – on a timescale that is large compared to the timescale on which x reaches its equilibrium. A small change Δp in p (see fig. 2.2) will tend to drive x from its equilibrium, but this is immediately followed by the return of x to its equilibrium (Δx in fig. 2.2) in a time that is much shorter than the timescale for the change in p.

Hence any excursion from equilibrium driven by the change in p is immediately restored and x will remain effectively on its equilibrium curve during the variation in p. However, this is impossible at the turning points of the curve $x_e(p)$ and there something special will happen: a catastrophe.

For instance, assume that x is on the upper branch of the equilibrium curve and that p decreases. As the turning point $x_e = \sqrt{b/3}$ is reached stability is lost and x can only follow the arrows and evolve on a short timescale towards the lower equilibrium branch. This transition will appear as a catastrophe, an almost discontinuous change. Suppose now that p starts to increase again. Then a second catastrophe will occur at $x_e = -\sqrt{b/3}$. Note that in the region where there are multiple solutions for x ($|p| < 2(b/3)^{3/2}$) there is hysteresis in the solutions for changing p: x "remembers" where it came from.

This simple example shows two things:

1. Catastrophic or almost discontinuous changes of a certain variable in a physical system as a result of a gradual change in an external force – or parameter – may be modeled within a framework of smooth equilibrium surfaces of the physical variable that contain *turning points* and therefore *multiple solutions* for some values of the external force.

2. This framework makes it possible to explain the time dependent behaviour of the variable without actually solving its evolution equation. In many applications one may not even know the full evolution equations, but only the equilibrium surfaces, the direction of the arrows and some relevant time scales.

In the language of catastrophe theory the parameter that varies gradually is called the 'control' parameter and the variable that undergoes discontinuous changes, the "behaviour" variable.

Before I proceed to some applications in astronomy I will explore point 2 somewhat further and show that in many cases it is not even necessary to make a full stability analysis.

Suppose that one knows the equilibrium curves for a problem. The p,x-space is divided into two or more regions by these curves. Suppose that one also knows the direction of the evolution arrows at one point in each region of the p,x-space. Then the evolution arrows must have the same direction in each region as the one arrow that is known, since an evolution arrow can only change sign at the equilibrium curves, where $\dot{x} = 0$. A branch of the equilibrium curve is only stable when the arrows at both sides point towards it. Therefore at every turning point of the equilibrium curve the stability must change sign. However, this is only strictly true for one behaviour variable.

The situation is more complicated when there is more than one 'behaviour' variable. In particular one must be very careful when one has a behaviour variable that is indicative for a whole function, for example the total magnetic energy of a magnetic field in a certain part of space. In a diagram displaying the value of this variable as a function of some parameter instability may only become worse at a turning point, i.e. one eigenmode more becomes unstable at that point. Here a full stability analysis is needed. An example of such a situation is given in the next section.

2.2. Applications in astronomy

A clear example of the use of catastrophe theory in astronomy is the Van Tend and Kuperus model [5, 6] for the filament eruption that – probably – causes the solar flare phenomenon.

A filament (see photo 1) appears dark in comparison with the surrounding corona because the plasma in it is denser and cooler than that of the corona ($T \approx 2 \times 10^4$ K and $n_e \approx 10^{11}$ cm^{-3} versus $T \approx 2 \times 10^6$ K and $n_e \approx 3 \times 10^9$ cm^{-3} for the corona in an active region). Van Tend and Kuperus model a filament as an electric current in the corona. The magnetic field lines around the current inhibit conductive heating of the plasma inside the filament by the surrounding coronal plasma and support the extra weight of the matter inside the filament. Kuperus and Van Tend show that because of the large inertia of the photosphere the current cannot penetrate into it and therefore the circuit is closed by a surface current at the photospheric boundary. This surface current may be represented by an equivalent 'mirror'-current in the photosphere.

The position of the filament is determined by three forces:

1. The current self-stress. It is well known that a closed current circuit wants to expand. In this case this results in an upward force on the filament because of the large inertia of the photosphere.

2. The mass-excess in the filament compared to its surroundings brings about a downward gravitational force.

3. There is an overall potential field in the corona with its sources in the neighbouring sunspots that gives rise to a Lorentz force on the filament. For the configurations of interest this force is downward.

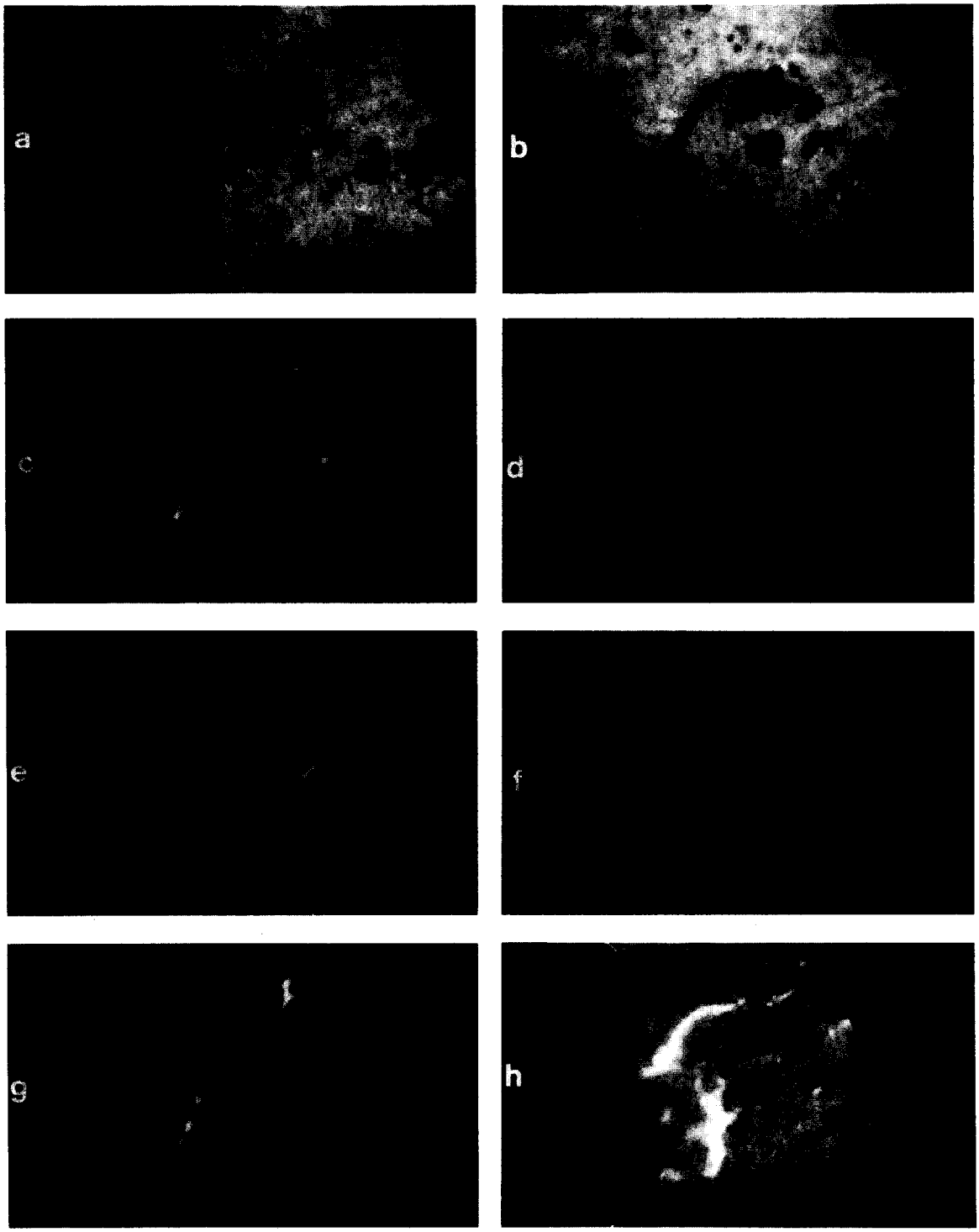

Photo 1. The filament eruption of the flare of May 16, 1981 as observed by the 53 cm Nikolsky type Coudé coronograph of Debrecen Observatory in Hungary. The time of observation of the series of photographs is in UT and the wavelength of observation is given relative to the Hα centre (6563 Å). a) 7:34, Hα + 1 Å; b) 7:58, Hα + 1 Å; c) 8:02, Hα + 0.5 Å; d) 8:02, Hα − 0.5 Å; e) 8:07, Hα + 0.5 Å; f) 8:07, Hα − 0.5 Å; g) 8:10, Hα + 0.5 Å; h) 8:26, Hα + 1 Å. The filament is the dark elongated absorption feature just left of the centre of the figure. The filament was located in active region Hale No. 17644 at 23° from the disk centre. Assuming a strict vertical ascent its increase in height could be calculated from the apparent displacement: from 7:57 to 8:12 its height increased from 24 000 to 62 000 km and at 8:10 the X-ray emission (observed by other instruments) started increasing. This filament eruption at the onset of the flare is consistent with the Van Tend and Kuperus scenario [5]. From F. Fárnik, B. Kálmán et al. [117]. Courtesy of Solar Physics and B. Kálmán.

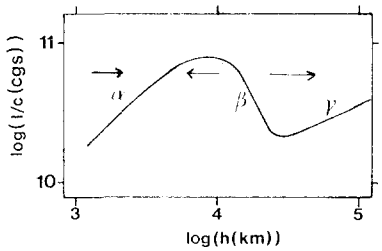

Fig. 2.3. The catastrophe picture for the filament eruption in the Van Tend and Kuperus model [5, 6]. From Van Tend [6]. Courtesy of the C.N.R.S. and the author.

For a given current I Kuperus and Van Tend calculate the equilibrium height h of the filament and the stability of the configuration. Figure 2.3 gives these equilibrium configurations together with the evolution arrows. One immediately recognizes the catastrophe picture. As the current – the control parameter – gradually increases the filament will rise and finally lose equilibrium at the end of the branch α and erupt to a new stable state on branch γ. These filament eruptions are actually observed in the solar corona at the onset of solar flares and the energy released is of the order of the flare energy. The sequence of pictures in photo 1 shows an example of a filament eruption.

The Van Tend and Kuperus model is phenomenological in the sense that they do not give – or attempt to give – a full solution of the MHD equations that govern the coronal magnetic field. For more than 10 years now solar physicists have been trying to derive analytically or numerically multiple solutions to the MHD equations that describe the coronal magnetic field. Once these multiple solutions are established the task is to find catastrophic transitions by slowly varying the photospheric boundary conditions of the coronal magnetic field. It is evident from the description of the filament eruption above such catastrophes are very well suited to explain solar flares, which as the observations indicate derive their energy from a sudden rearrangement of the coronal magnetic field.

Low [7] has recently given an excellent review of the large amount of work that has been done along these lines. The basic problem he describes is as follows. Because of the dominance of the magnetic pressure over the gas pressure in active regions in the corona, the magnetic field must be evolving on a very fast time scale (the MHD time scale, which is of the order of the dimension of the region of interest divided by the Alfvén speed; a few seconds under typical coronal conditions) or it must be in a force-free state governed by ($\boldsymbol{B}$ is the magnetic field)

$$(\nabla \times \boldsymbol{B}) \times \boldsymbol{B} = 0 \tag{2.2.1}$$

$$\nabla \cdot \boldsymbol{B} = 0 . \tag{2.2.2}$$

The electric currents ($\boldsymbol{J} = (1/4\pi)\nabla \times \boldsymbol{B}$) carry the free energy necessary to fuel a flare.

Because of the well-known 'frozen-in' condition of astrophysical plasmas the field lines are anchored in the photosphere where the gas pressure dominates over the magnetic pressure and hence the footpoints of the coronal field lines are forced to follow the photospheric motions. The coronal magnetic field readjusts very quickly to these generally slow changes in footpoint positions and hence the field evolution is essentially a sequence of force-free equilibria having the same topology as long as there is no field reconnection.

In terms of catastrophe theory the photospheric boundary conditions represent the control variables

and the coronal magnetic field structure is the behaviour variable. A necessary condition for the occurrence of catastrophic transitions in that the sequence of force-free equilibria contains a turning-point (or end-point), which is in principle possible because of the non-linearity of the force-free equations (2.2.1) and (2.2.2).

Low [7] in his review paper indeed gives some completely analytical examples of such topologically invariant sequences of force-free equilibria. However, despite these important achievements the problem still does not seem to be settled satisfactorily because the constructed examples either contain unphysical singularities or the turning-points cannot be reached merely by footpoint motions, that is the turning-points can only be approached as a limit by infinite footpoint displacements.

A serious limitation to the use of catastrophe theory in solving the flare problem is further that it is not possible to predict exactly to which new equilibrium configuration the magnetic field will evolve since the impulsive heating of the plasma – which is characteristic of flares – requires the dissipation of currents and therefore a temporary violation of the force-free and frozen-in conditions of the field. Without going into the details of the time dependent MHD equations it seems difficult to predict just how much current is going to be dissipated and thus consideration of (sets of) equilibria alone – as in catastrophe theory – does not give an answer to the question how much energy is released in the flare. There is an obvious upper limit however to the amount of energy released in a flare and that is the difference in energy content of the field before the catastrophe and that of a potential field satisfying the same boundary conditions. (The potential field is the configuration with minimum energy for given boundary conditions.)

The solar corona is also the setting for two other catastrophic transitions which occur in the thermal structure of so-called coronal loops. Coronal loops are the loop-like structures that are clearly visible in X-ray pictures of the solar corona (see photo 2). The plasma in these loops is much denser and somewhat hotter than that of the surrounding corona and this makes them radiate more intensively in X-rays, since the radiative losses for an optically thin plasma at coronal temperatures increase with the square of the density. Elementary considerations show that there must be local mechanical heating to make up for the radiative losses.

Conduction of heat across the field lines is greatly inhibited, but the conductivity along the field is very large for a plasma at coronal temperatures. This leads to a one-dimensional description of the energy balance of the plasma in which three terms dominate: heating, conduction and radiative losses. Solution of the static energy balance – as was first done by Rosner, Tucker and Vaiana [8] – leads to two so-called scaling laws

$$T_{\max} \approx 1400(PL)^{1/3} \qquad \text{[c.g.s.]} \tag{2.2.3}$$

$$E_{\mathrm{H}} \approx 10^5 P^{7/6}/L^{5/6} \qquad \text{[c.g.s.]}\,. \tag{2.2.4}$$

Here $T_{\max}$ denotes the maximum temperature in the loop, L the *half*-length of the loop, E_{H} the local heating rate (assumed to be constant over the loop) and P the pressure that is also assumed to be constant because at typical loop temperatures ($\approx 2 \times 10^6$ K) the pressure scale height is larger than the typical loop height. The temperature structure in the loop is that of a nearly isothermal hot part in the corona bounded by two sharp transition regions at the footpoints where the temperature drops within a few hundred kilometers to about 20 000 K (for comparison: a typical value for L is 30 000 km).

Hood and Priest [9, 10] while performing numerical calculations on the temperature structure of coronal loops, first noted that there exists the possibility of a second, relatively cool ($T \approx 20\,000$ K)

Photo 2. The Sun in X-rays on November 27, 1973, 1:44 UT. This picture is a 64 sec exposure with the soft X-ray telescope SO V aboard Skylab, taken through a filter with a bandpass of 2–32, 44–54 Å. North is towards the upper right corner. Clearly visible are a few active regions, where the magnetic field has broken out the solar interior. There are several loop-like structures visible that are somewhat less bright than the active regions themselves. Note for example the set of loops beneath the large active region just left of the centre of the disk. The X-rays are caused by optically thin thermal radiation from a plasma with a temperature of a few million degrees and a density of 10^9–10^{10} cm^{-3}. The plasma in the loops is heated by the dissipation of currents which are generated and maintained by electrodynamic coupling with the underlying photosphere (Ionson [14]). Courtesy of the Solar Physics Group, American Science and Engineering, Inc., Cambridge, Massachusetts 02139, U.S.A.

equilibrium in which heating locally balances radiative loss and in which conduction plays no role. Using alternatively the loop length, the amount of heating and the pressure in the loop as 'control' variables Hood and Priest showed the occurrence of catastrophic transitions between the 'hot' and 'cool' states of coronal loops.

Martens and Kuin [11] pointed out that the assumption of constant pressure is not correct for the cool loops and that consequently the pressure of the loop cannot be used as a control variable – because it is not an independent variable – and that changes in the heating rate neither trigger catastrophes. A catastrophic transition from the 'cool' to the 'hot' state remains possible however as the height of the top of the loop in the corona surpasses a certain threshold value. The loop geometry is determined by the magnetic field so it is the evolution of the latter that triggers the thermal catastrophe.

The thermal equilibrium in the 'cool' loops is determined by energy balance and pressure balance,

resp.

$$E_H = P^2 \chi(T) \tag{2.2.5}$$

$$\frac{1}{P}\frac{dP}{dh} = -\frac{g}{2RT}. \tag{2.2.6}$$

The same symbols as in (2.2.3 and 4) are used. E_H is assumed constant for simplicity. $\chi(T)$ is the radiative loss function for an optically thin plasma of solar composition at constant pressure, as calculated by McWirther et al. [12] and Raymond et al. [13] (see fig. 2.4). h is the height above the transition region, g is the gravitational acceleration and R is the gas constant.

Eq. (2.2.5) determines a relation between pressure and temperature in the loop that may be used to draw an equilibrium curve in a P, T-diagram, fig. 2.5. This curve contains a turning point corresponding to a sharp peak in radiation losses at about 20 000 K (see fig. 2.4). Eq. (2.2.6) merely expresses the well-known fact that the pressure in the loop decreases as the height increases. There is however a minimum pressure for thermal equilibrium as fig. 2.5 indicates and when the top of the loop surpasses the height corresponding to that pressure the 'cool' equilibrium is no longer possible because thermal equilibrium and pressure balance cannot be satisfied at the same time. The plasma in the loop will heat up since $E_H > E_R$ at the top and this decreases the radiation loss and makes the plasma heat up further. There is no new equilibrium at higher temperatures between heating and radiation losses and therefore the temperature increase continues until another term comes into play in the energy balance: conduction. The new equilibrium configuration between heating, conduction and radiative losses is indicated in the figure. This is the hot loop described by the scaling laws (2.2.3) and (2.2.4).

The catastrophe picture of fig. 2.5 is that of an imperfect catastrophe: a catastrophe may be predicted but the new equilibrium is not described by the same equations as heat conduction becomes important and therefore cannot be indicated by continuation of the equilibrium curve in the figure.

Changes in the length or magnetic field strength (resp. L and B) of a coronal loop may also lead to

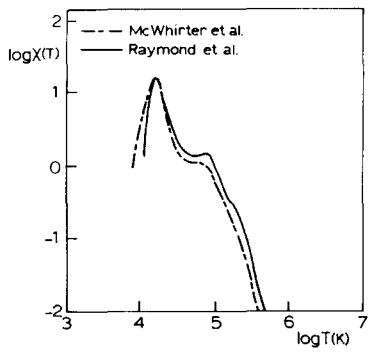

Fig. 2.4. The radiation loss curve for an optically thin plasma at constant pressure. $\chi(T)$ is expressed in $cm^3\,erg^{-1}\,sec^{-1}$. From Martens and Kuin [11].

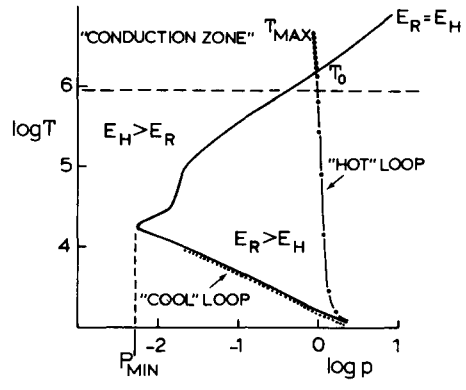

Fig. 2.5. The $\log P$–$\log T$ diagram for loop models with constant heating per unit volume, $E_H = 4 \times 10^{-4}\,erg\,cm^{-3}\,sec^{-1}$. The drawn line is the curve where the heating equals radiative losses. The radiative loss curve of Raymond et al. [13] is used. The stable cool loops lie along the lower branch of the drawn curve. The solution for 'hot coronal loops' is also indicated. The dots in both solutions represent points in the loop at equal distances. From Martens and Kuin [11].

catastrophic transitions between different 'hot' states of the loop plasma. The heating of these loops has recently been described by Ionson [14] in terms of electrodynamic coupling between the loop structure and the underlying photosphere. Ionson shows that there is a close mathematical analogy between a coronal loop and an LRC circuit with a high quality factor. The footpoints of the loop are anchored in the photospheric plasma and because of the high density there they are forced to follow photospheric motions. Standing MHD waves with a period equal to the resonance period of the loop build up as a result of periodic footpoint motions until the wave energy entering the loop is matched by the energy dissipated in it, which causes the heating of the plasma. The resonance frequency ν of a loop is given by the time it takes for an Alfvén wave to travel from one footpoint to the other and back – after reflection at the photospheric boundary. Thus

$$\nu = \frac{V_A}{4L} = \frac{B}{8\sqrt{\pi\bar{\rho}}\, L} \tag{2.2.7}$$

where $\bar{\rho}$ is the mean density in the loop.

From the energy available in the photosphere the loop picks out one small frequency interval around the resonance frequency and absorbs all the energy in that band and no energy at other frequencies – just as an LRC circuit. The heating rate does not depend on the bandwidth of absorption, a feature which is also known from LRC circuits. It depends on the photospheric power spectrum in the following way (Ionson [14] eq. 61)

$$E_H(\nu) \approx 10^{13} S(\nu)/L^2 \qquad [\text{erg cm}^{-3}\,\text{sec}^{-1}] \tag{2.2.8}$$

where $S(\nu)$ is the photospheric power spectrum. Working back from the observations of magnetic field, temperature and density in hot coronal loops, Ionson found that the power spectrum must have two definite peaks, one at the frequency of the chromospheric three minute oscillation and one at the convective turn-over time ($\approx$800 sec). Loops with the corresponding resonance frequencies are strongly heated and therefore clearly visible in X-rays, while loops at different resonance frequencies are observed to be somewhat cooler and much fainter.

Martens and Kuperus [15, 16] use the definition of resonance frequency (2.2.7), the gas law and the scaling laws (2.2.3 and 4) to express the overall radiation losses in a hot loop as a function of the resonance frequency alone, with the loop length and magnetic field strength as external parameters

$$E_R(\nu) \approx \frac{730 B^{7/2}}{L^{15/4} \nu^{7/2}} [\text{erg cm}^{-3}\,\text{sec}^{-1}]\,. \tag{2.2.9}$$

It is easily shown that there cannot be an appreciable conductive flow across the chromospheric boundary of a hot loop in a static situation (e.g. Martens and Kuin [11]) and therefore the loops are effectively thermally insulated. Thermal equilibrium is then reached when the *overall* heating balances the overall radiation loss since conduction only displaces energy within the loop. Thus

$$E_H(\nu) = E_R(\nu) \tag{2.2.10}$$

defines the overall thermal equilibrium of a hot coronal loop: conduction is important in the *local* energy balance but for the loop as a whole all the heating must be radiated away.

Both observations and numerical calculations show that when out of thermal equilibrium, the loop plasma evolves according to the 'evaporation/condensation' scenario (Krall and Antiochos [17], Craig and McClymont [18]).

According to this scenario a rise in coronal temperature leads to an excess conductive flux into the transition region. This flow reaches the base of the transition region but cannot penetrate into the chromosphere because of the low thermal conductivity there. What happens is that a layer at the base of the loop is heated up impulsively to coronal temperatures and that this material is then redistributed over the loop. The resulting increase in mean loop density causes an increase in radiative losses and a subsequent return to equilibrium by radiative cooling.

The opposite occurs when the loop temperature falls below its equilibrium value. Now the conductive flow into the transition region becomes too small to keep it radiating statically and some material must cool down: condensation. The resulting decrease in density leads to a decrease in radiative losses, heating up of the loop plasma and a return to equilibrium.

Without this coupling between coronal and chromospheric plasma the coronal plasma would be radiatively unstable because at coronal temperatures a temperature increase leads to a decrease in radiative losses and vice-versa.

The 'evaporation/condensation' scenario may be formalized with the expression

$$\mathrm{d}\bar{p}/\mathrm{d}t \sim E_{\mathrm{H}} - E_{\mathrm{R}} \tag{2.2.11}$$

where $\sim$ denotes equality of sign. Noting the relation between $\bar{p}$ and ν, eq. (2.2.7), I may write

$$\mathrm{d}\nu/\mathrm{d}t \sim E_{\mathrm{R}}(\nu) - E_{\mathrm{H}}(\nu) \tag{2.2.12}$$

which defines the direction of the evolution arrows in fig. 2.6. The external parameter in this catastrophe picture is L/B^2.

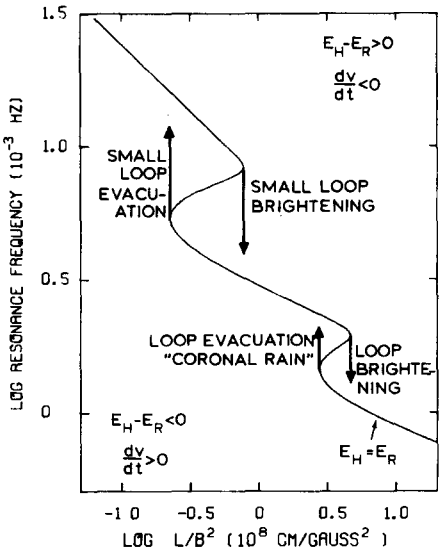

Fig. 2.6. The equilibrium resonance frequency of a coronal loop as a function of the parameter loop length divided by magnetic field strength squared. When L/B^2 changes slowly compared to the radiative cooling time of the loop plasma the loop evolves along the curve of thermal equilibria until one of the turning-points is reached: then a thermal catastrophe occurs of the type that is indicated in the figure. From Martens and Kuperus [15].

Two catastrophes are possible, which lead to changes in the resonance frequency that imply changes in the heating rate of about a factor 8. Therefore a slow increase in the loop length or a slow decrease in magnetic field strength can lead to a sudden increase of heating and consequently of X-ray emission of the loop. The most probable time scale for this transition is the thermal time scale (the thermal energy content of the loop divided by the total heating rate) which is about 20 minutes for typical solar coronal loops. This is just what has been observed in Skylab X-ray movies as photo 3 shows. See Howard and Svestka [19] for a description.

The reverse catastrophe – the sudden disappearance of bright X-ray loops – has also been observed (e.g. Levine and Withbroe [20]) and was named 'loop evacuation' because the plasma in the loop was

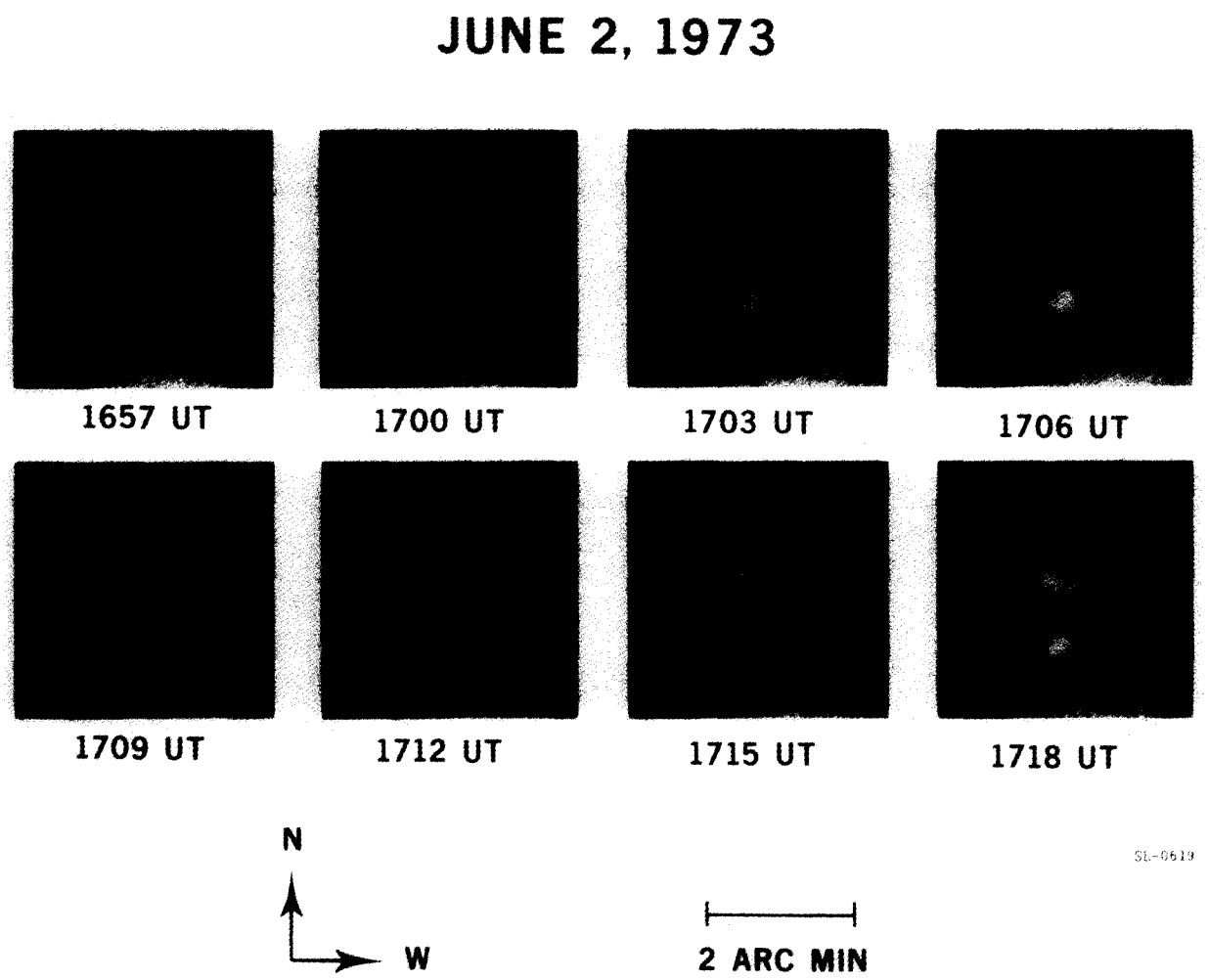

Photo 3. Skylab X-ray observations of the brightening of two coronal loops. The X-ray image was recorded by the S-054 telescope with a 16 sec exposure taken through a filter having a bandpass of 2–32, 44–54 Å. These loop brightenings are consistent with the scenario for thermal catastrophes in resonantly heated coronal loops of Martens and Kuperus [15]. From Solodyna et al. [118]. Courtesy of the Solar Physics Group, American Science and Engineering, Inc., Cambridge, Massachusetts 02139, U.S.A.

observed to be falling into the chromosphere when cooling (due to loss of buoyancy). The 20 minutes duration of the events is confirmed by the observations (e.g. photo 3) and also by recent calculations of Martens and Kuin [21] who used a time dependent formalism to describe the loop plasma instead of the static scaling laws.

From a completely different field comes the work of Hut [22] on the dynamical evolution of a binary system under the influence of tidal forces. Hut uses the fact that the total angular momentum of the binary system is rigorously conserved and that its total energy cannot but decrease under the influence of tides. In this way the equilibrium solutions for the binary and the direction of the evolution arrows of the system can be found without the need to solve – or even write down – the detailed evolution equations. Only sequences of equilibrium configurations need to be considered. For the restricted case of a circular coplanar orbit, the situation is nicely condensed in one drawing, fig. 2.7. The stars must move on a line of constant L (total angular momentum) and the equilibria and evolution arrows as a result of tidal interaction are indicated. a is the distance between the stars. Clearly only for a limited number of initial values stable coplanar and corotating solutions are possible. Stability only occurs when the orbital angular momentum exceeds the sum of the spin angular momenta by more than a factor of about three. Unstable orbits lead to coalescence of the binaries or to disruption due to the strong centrifugal forces in the stars as $a \to 0$.

A final example of 'catastrophysics' is the gravothermal catastrophe of Antonov [23] and Lynden-Bell and Wood [24] that has been recently extended by Katz [25] and Demaret et al. [26]. The thought experiment originally conceived by Antonov [23] is as follows: consider a large number of mass points (stars) moving inside a perfectly reflecting sphere with a given radius. The gas (of stars) in the sphere is considered to be isothermal because the time scale for conductive energy transport is much smaller than the time scale for the change in any external parameter. The only relevant interaction between the particles is their mutual gravitational attraction. Antonov considered a series of equilibria for the gas in the spheres with constant total mass and energy (gravitational potential plus thermal) and varying radius and found that gravitational collapse takes place when the radius surpasses the critical value $R_c = 0.355GM^2/(-E)$ where M is the total mass of the particles, E the energy of the gas and G the gravitational constant. As the particles condense in the centre of the sphere the temperature of the gas increases indefinitely. This process is only stopped when the present description of the gas is not valid anymore (e.g. because radiative losses come into play). This result was extended by Lynden-Bell and

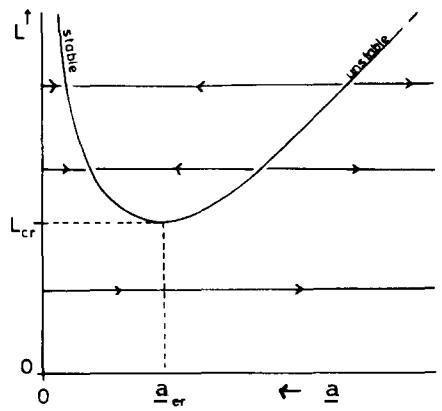

Fig. 2.7. Angular momentum versus distance for coplanar binaries in a circular orbit. The arrows indicate the evolution of the binary system under tidal friction. This figure is from Hut [22]. Courtesy of Astronomy and Astrophysics and the author.

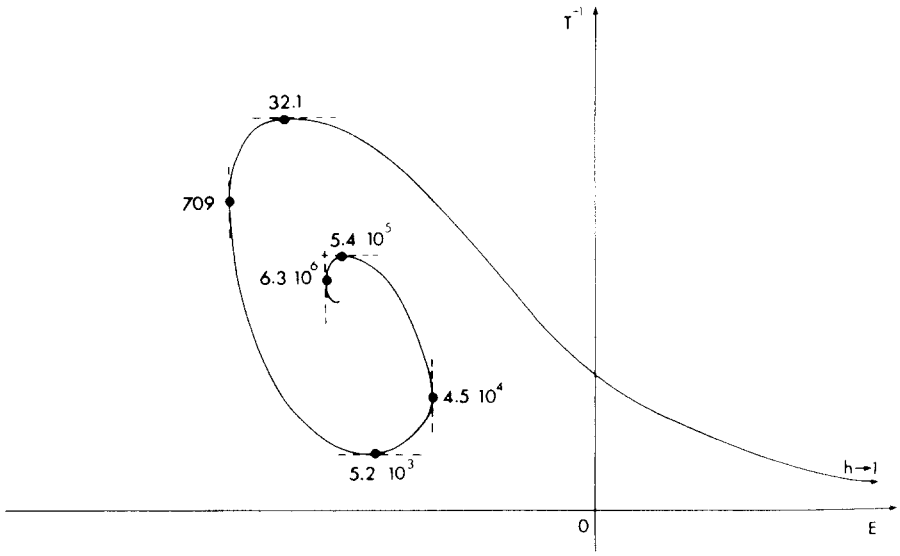

Fig. 2.8. Inverse temperature versus total energy for isothermal spheres of constant mass and volume. h is the ratio between the density in the centre and that at the surface of the sphere. At $h = 709$ the first eigenmode becomes unstable and at subsequent turning-points more and more modes follow. This figure is from Katz [25]. Courtesy of Monthly Notices and the author.

Wood by also considering a 'plastic' sphere (i.e. a sphere in pressure equilibrium with its surroundings) and spheres in a 'heath bath' that keep the same temperature instead of constant energy. The catastrophe picture, fig. 2.8 giving a series of equilibria for a sphere with constant mass and volume and varying total energy, shows that this gravothermal catastrophe has a topology that is different from that of the examples above. Here the "behaviour" variable (T^{-1}) is indicative of a whole function: the density distribution within the sphere. The sequence of thermal equilibria, starting at $h = 1$, is stable until it loses stability at the first turning-point ($h = 709$). At the second turning-point ($h = 4.5 \times 10^4$) a second eigenmode of the linear differential equations describing small perturbations of the equilibrium state becomes unstable and hence the sequence of equilibria remains unstable. This continues ad infinitum: at each turning-point one more eigenmode becomes unstable.

This example is a demonstration of the caution that has to be taken when the behaviour variable represents a whole function. In that case a turning-point does not imply interchange of stability.

3. Bifurcations

3.1. Ordinary bifurcations

Let us consider again the model eq. (2.1.1). Now I allow for variations in b and take $p = 0$:

$$\dot{x} = bx - x^3 . \tag{3.1.1}$$

For all values of b this equation has the static solution $x = 0$ and for $b > 0$ there are two other solutions, $x_e = \pm\sqrt{b}$. Using the method of first order perturbations it is immediately found from (3.1.1) that the

solution $\dot{x} = 0$ is stable for $b \leqslant 0$ and unstable for $b > 0$. For the solutions $|x| = \sqrt{b}$ one finds ($\varepsilon = x - x_e$)

$$\dot{\varepsilon} = -2\varepsilon b \tag{3.1.2}$$

which implies stability. These results are summarized in the bifurcation diagram fig. 3.1. Just as in the previous section the arrows indicate the direction of the evolution. As b increases slowly compared with the time scale needed for a solution to reach the equilibria curve the solution will remain on this curve (just as in the example for catastrophes). At $b = 0$ the static solution changes its character as is evident from fig. 3.1. This example is about the simplest that can be given for a bifurcation. A bifurcation is always connected with the loss of stability of a static solution caused by the change in some external parameter. When the original static solution gives way to a new – not necessarily stable – equilibrium that branches off at the point of loss of stability, this is called a bifurcation. More precisely, in the words of Iooss and Joseph [27]: 'Bifurcations are equilibrium solutions which form *intersecting* branches in a suitable space'.

The theory of bifurcations is not particularly new. Already in 1834 Jacobi studied a bifurcation in the equilibrium of self-gravitating rotating bodies [28] and he introduced the word "Abzweigung". Poincaré introduced the French word 'bifurcation' in 1885 in a study on the same subject [29]. Many reviews and books have appeared since. A fairly recent one and also comprehensible for non-mathematicians is the review by Stakgold [30]. Iooss and Joseph present an introduction at the undergraduate level [27]. What is new in the theory of bifurcations is the realisation of the decisive role that may be played by bifurcations in the onset of chaotic behaviour. This will be the subject of section 4.

There are many types of bifurcations but in this review I shall only give some examples of the bifurcations that are important in connection with the other sections. To establish the connection with catastrophe theory I proceed with eq. (2.1.1) and now analyse the case $p \neq 0$. Suppose $p > 0$. The static solutions are given by

$$b = x_e^2 - p/x_e\,. \tag{3.1.3}$$

This is illustrated in fig. 3.2. For $p' = -p$ the same figure is obtained for $x_e' = -x_e$, so nothing is lost by the restriction to positive p. Figure 3.3 shows the corresponding solution of x as a function of b. Again the evolution arrows may be obtained easily and thereby one finds the stable and unstable branches. It is evident that the bifurcation has vanished: the equilibrium solutions no longer intersect. For small p this is called an 'imperfect' bifurcation. The same figure might have been obtained by taking a cross section of constant p in fig. 3.4, which gives the equilibrium surfaces in x,p,b-space. The point in

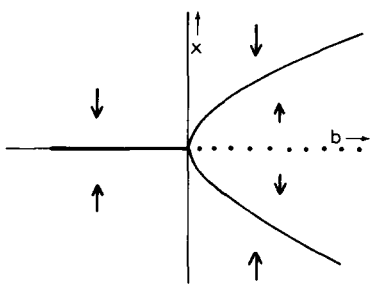

Fig. 3.1. The supercritical bifurcation.

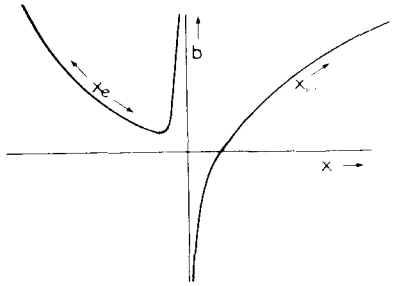

Fig. 3.2. The solution of eq. (3.1.3).

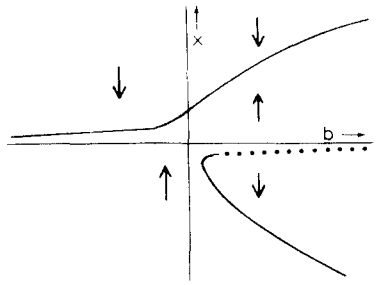

Fig. 3.3. The imperfect bifurcation.

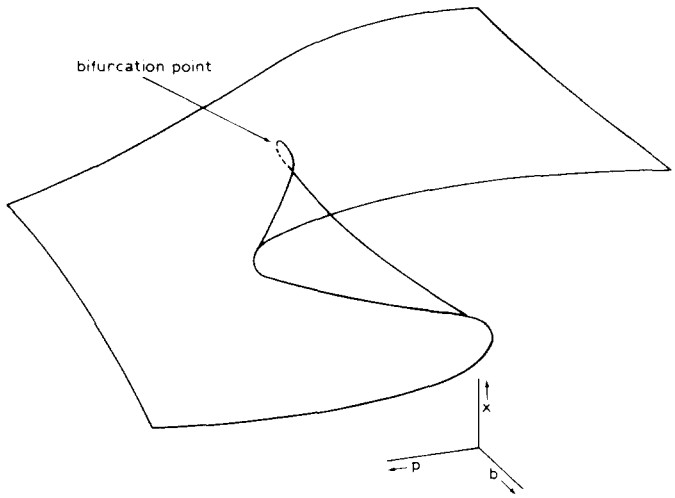

Fig. 3.4. The equilibrium surface of eq. (2.1.1) in x,p,b-space.

showing this is to illustrate how in many actual physical systems one side of a bifurcation is preferred, because of small imperfections in the system. For example consider a straight *elastic* column under an end load b as indicated in figs. 3.5 and 3.6 (this example comes from Iooss and Joseph [27]). When the load increases the completely straight column in fig. 3.5 may eventually buckle either to the right or to the left, but a slightly bent column, such as the one in fig. 3.6 will buckle to the left. The bifurcation diagrams of these bucklings are similar to figs. 3.1 and 3.3 respectively.

In fig. 3.3 a catastrophe is possible for a solution along the lower branch as b decreases, but the reverse catastrophe cannot happen. Only after a *finite* perturbation in the equilibrium along the upper branch, large enough to bring x in the domain bounded by the unstable solution a jump to the other

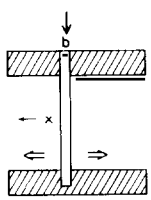

Fig. 3.5. The buckling of a straight elastic column. No preference.

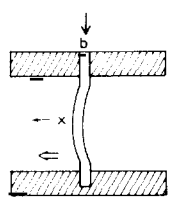

Fig. 3.6. The preferential buckling of a bent elastic column.

branch is possible. Note that in the surface of x_e in x,p,b-space there is only one real bifurcation at the origin.

The analysis of perfect bifurcations is continued by considering a slightly more complicated version of (3.1.1)

$$\dot{x} = bx + 2ax^2 - x^3 . \tag{3.1.4}$$

The static solutions are

$$x_{e,1} = 0 ; \qquad x_{e,2,3} = a \pm \sqrt{a^2 + b} . \tag{3.1.5}$$

The last two solutions appear when $b \leqslant -a^2$. These solutions and their stability are given in fig. 3.7. The solution that intersects the solution $x_e = 0$ at $b = 0$ now exists on both sides of the line $b = 0$. This is called a two-sided or *transcritical* bifurcation, in contrast to the example in fig. 3.1, which is a *supercritical* bifurcation. Note the subtle differences with the imperfect bifurcation, fig. 3.3. The transcritical bifurcation is actually the simplest bifurcation, since locally – i.e. in the neighbourhood of the bifurcation point – it involves a quadratic non-linear term instead of only a cubic one. The quadratic term is in general the lowest order non-linear term that is obtained in a series expansion of the evolution equation around a certain static solution.

Finally I demonstrate the *subcritical* bifurcation. Consider the evolution equation

$$\dot{x} = bx + 2ax^3 - x^5 . \tag{3.1.6}$$

As in the previous examples there is a static solution $x_e = 0$ that changes stability at $b = 0$. When $a < 0$ and close to the bifurcation point, the fifth-order term in (3.1.6) is of no interest and the problem may be reduced to the form (3.1.1) by a trivial transformation. For $a > 0$ the third-order term contributes to the instability and one needs to include the higher-order terms to find the bifurcating solution. The equilibrium solutions, apart from $x_e = 0$, are defined by

$$b = x_e^4 - 2ax_e^2 . \tag{3.1.7}$$

Using this one easily finds the bifurcation diagram, fig. 3.8. As usual the stable and unstable branches and the evolution arrows are indicated.

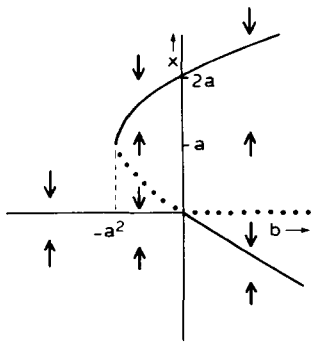

Fig. 3.7. The transcritical bifurcation.

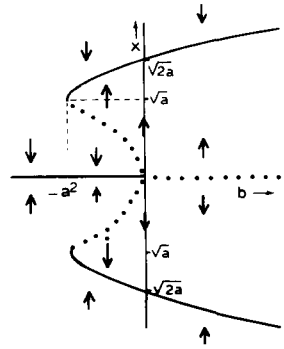

Fig. 3.8. The subcritical bifurcation.

In this example again the possibility of *hysteresis* with changes of the parameter b is encountered. This hysteresis curve is slightly more complicated than the one in fig. 2.2, but the topology of the hysteresis loop, for example in the north-west quadrant, is the same as that for the catastrophe curve.

3.2. Hopf bifurcations and limit cycles

So far I have only considered bifurcations in evolution equations for one variable. When this study is extended to the case of two or more variables the possibility of a *periodic* solution branching-off is encountered. This is called a Hopf bifurcation, after E. Hopf, who gave a clear demonstration of this phenomenon in 1942 [31].

Again I will demonstrate this bifurcation from a simple example. Consider the system of evolution equations

$$\begin{aligned} \dot{x} &= -y + bx - x^3 - y^2 x \\ \dot{y} &= x + by - y^3 - x^2 y\,. \end{aligned} \tag{3.2.1}$$

For any value of b a static solution of this system is $x_e = y_e = 0$. It can be shown that there are no other static solutions of (3.2.1). The solution for the linear part of (3.2.1) for some given initial values x_0 and y_0 is

$$\begin{aligned} x(t) &= x_0\, e^{bt} \cos t - y_0\, e^{bt} \sin t \\ y(t) &= y_0\, e^{bt} \cos t + x_0\, e^{bt} \sin t\,. \end{aligned} \tag{3.2.2}$$

This represents a damped oscillatory solution for $b < 0$. Evidently the static solution loses stability as b increases from negative to positive values: the system now starts to oscillate with an increasing amplitude. As before one might expect a stable static solution branching-off, but examination of (3.2.2) reveals that the period of the oscillations remains unchanged as b increases and moreover there are no static solutions apart from the 'null' solution. The alternative is that an oscillatory solution branches-off and grows in amplitude until the non-linear terms prohibit further growth. Whether this really happens depends on the precise form of the non-linear terms, just as in the case of an ordinary bifurcation.

In example (3.2.1) a cyclic solution does indeed branch-off and this may be verified by a complete solution of the system. For this purpose change to polar coordinates

$$\begin{aligned} r^2 &= x^2 + y^2 \\ \psi &= \arctan(y/x)\,. \end{aligned} \tag{3.2.3}$$

One easily obtains with the use of (3.2.1)

$$\begin{aligned} \dot{r} &= br - r^3 \\ \dot{\psi} &= 1\,. \end{aligned} \tag{3.2.4}$$

Hence the stationary solution for $b > 0$ is

$$r = \sqrt{b}$$
$$\psi = \psi_0 + t. \tag{3.2.5}$$

By perturbing this solution it is found that the amplitude of the oscillation is stable and that the solution is insensitive to small phase shifts. The bifurcation diagram, fig. 3.9, in the three-dimensional x,y,b-space is that of a straight line intersecting head-on a paraboloide. As in the previous examples the stability of the 'null' solution (the line) changes sign as it intersects the other equilibrium curve. Because of the cylindrical symmetry it suffices to consider a projection on a plane ψ = constant and thus the bifurcation diagram, fig. 3.1 is recovered.

For a given positive value of b the solutions in the x,y-plane spiral towards the circle $r = \sqrt{b}$, that is called the *limit cycle*, because it attracts all solutions. See figs. 3.10 and 3.11.

A Hopf bifurcation is always associated with a degeneracy in the problem that is treated. When the

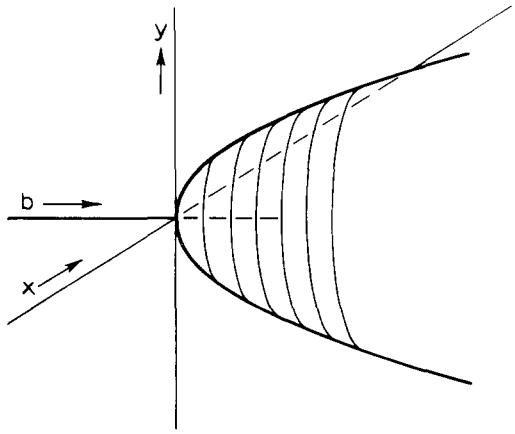

Fig. 3.9. The supercritical Hopf bifurcation.

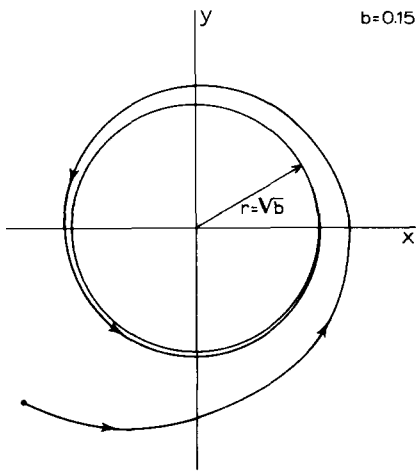

Fig. 3.10. The solution of eq. (3.2.1) with an initial value outside the limit cycle.

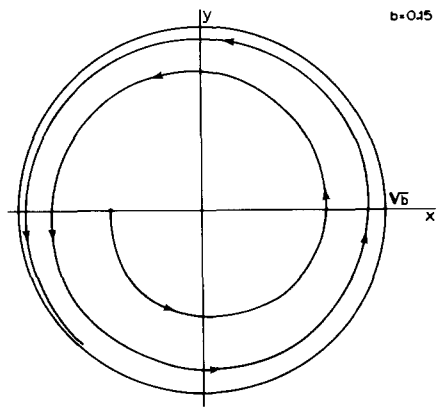

Fig. 3.11. The solution of eq. (3.2.1) with an initial value inside the limit cycle.

evolution equation contains only real coefficients the dispersion matrix for small amplitude perturbations to the static solutions yields only *real* or *complex conjugated* eigenvalues. A Hopf bifurcation occurs when the real part in a pair of complex conjugated eigenvalues changes sign and thus at least *two* eigenvectors simultaneously turn unstable, which is degeneracy. When a real eigenvalue changes sign an ordinary bifurcation takes place.

Hopf bifurcations may be classified just like ordinary ones. It can be shown that there is no transcritical Hopf bifurcation, which is caused by the degeneracy of the problem (for a proof, see [27] Chap. 7). Thus only the subcritical and supercritical Hopf bifurcations remain (cf. figs. 3.1 and 3.8).

For the subcritical Hopf bifurcation there is again the possibility of hysteresis, with the two coexisting solutions now being a point attractor and a limit cycle. For a given value of b in the hysteresis region the solution in the x,y-plane is depicted in fig. 3.12. The region of initial values that lead to the point solution is separated from the rest of the plane by a *separatrix* or *repelling* cycle. The radius of both cycles as a function of b can be found in comparing with fig. 3.13, which gives the bifurcation diagram for a Hopf bifurcation defined by the equations

$$\dot{r} = br + 2ar^3 - r^5$$
$$\dot{\psi} = 1 . \tag{3.2.6}$$

For slowly increasing b the static solution may catastrophically change into an oscillating one with finite amplitude and for decreasing b a stable cyclic solution may suddenly disappear and give way to a static solution. Figure 3.8 represents a cross section at constant ψ of fig. 3.13.

The stability of the periodic solution that branches-off in a Hopf bifurcation is investigated with the use of the Floquet theory, a generalised form of the usual perturbation analysis [27, Chap. 7]. The examples of this section are so simple that a separation of variables is possible and stability is evident, but in more complicated situations this is not so and then one has to use Floquet theory.

It is clear from the above discussion that a Hopf bifurcation may lead to a *limit cycle*. When for a given differential equation all solutions converge to a periodic one – in a certain domain of initial

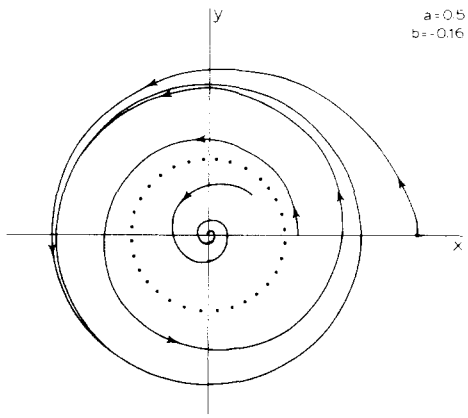

Fig. 3.12. Solution curves after a subcritical Hopf bifurcation (eq. (3.2.6)). The dotted curve represents the separatrix, the full curve the limit cycle.

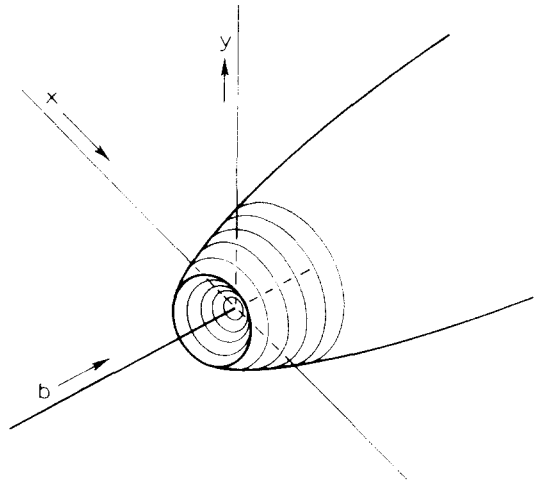

Fig. 3.13. The subcritical Hopf bifurcation.

conditions – this solution is called a periodic attractor and its representation in phase space is a limit cycle. Evidently in this case the phase space must be at least two-dimensional. Equations for one degree of freedom have only stable static solutions as attractors: point attractors.

In the neighbourhood of point and periodic attractors the governing equations are dissipative – i.e. a volume in phase space must shrink continuously – so the solutions tend towards a curve of lower dimensionality as the phase space. Hence no attractors will be found in the conservative equations of motion. Adding an energy sink term in these equations – e.g. a damping term in the equations for the harmonical oscillator – generally leads to the emergence of a point attractor, describing the rest situation of the system. Adding still other terms representing energy sources further complicates the situation and may lead to both point and periodic attractors. In general attractors – including the strange attractors of the next chapter – arise in equations for open systems, i.e. systems with energy sinks and energy sources.

3.3. Bifurcations in partial differential equations

So far I have treated bifurcating solutions in ordinary differential equations. They may be suggestive with respect to phenomena that are encountered in continuous physical systems, like fluids or gases, but no more than that, because these systems are described by *partial* differential equations.

The Rayleigh–Bénard experiment is an example that has obvious importance for astrophysics. It is extensively described by Busse, both from the theoretical and experimental point of view and with emphasis on the development of turbulence [32]. In the Rayleigh–Bénard experiment a fluid layer is heated from below, so that the top and the bottom of the fluid layer are kept at a constant, but different temperatures. The temperature of the bottom of the fluid is the higher one. For small temperature differences there is no motion in the fluid and the heat transport takes place by conduction. As the temperature difference between the top and the bottom is increased steady convective cells appear when the Rayleigh number of the system, which is a non-dimensional measure for the temperature difference between the upper and lower boundary (see eq. (4.3.4) for a definition), exceeds a certain critical value. This onset of convection is clearly suggestive of a bifurcating (supercritical) solution, because the "amplitude" of the convection is very small for Rayleigh numbers that are only slightly larger than the critical value.

The question to be addressed is, do bifurcations actually occur in the equations that describe Rayleigh–Bénard convection and in other equations that exhibit similar phenomena, like the Navier–Stokes equation? The answer is yes and many examples are given in 'Hydrodynamic Instabilities and the Transition to Turbulence' [33], which contains selected papers written by experts in various areas of fluid dynamics. Bifurcations are actually very common in partial differential equations. I will continue in the spirit of the previous sections by demonstrating a simple example.

Consider the equation

$$\partial u/\partial t = \partial^2 u/\partial x^2 + bu - u^3 \tag{3.3.1}$$

for the function $u = u(x, t)$. This equation has to be solved for $t > 0$ and $0 \leq x \leq 1$, with prescribed boundary conditions $u(0, t) = u(1, t) = 0$ and initial data $u(x, 0) = f(x)$, where $f(x)$ is some arbitrary function, satisfying the boundary conditions. The static solutions satisfy

$$\partial^2 u_e/\partial x^2 + bu_e - u_e^3 = 0\,. \tag{3.3.2}$$

It is easily verified that $u_e = 0$ is a static solution. To investigate the stability of this solution I note that any function $y(x)$ in the domain [0, 1] satisfying the boundary conditions may be decomposed in Fourier modes as

$$y(x) = \sum_{n=1}^{\infty} a_n \sqrt{2} \sin(n\pi x) . \tag{3.3.3}$$

The amplitude of the nth Fourier component is calculated by

$$a_n = \int_0^1 y(x) \sqrt{2} \sin(n\pi x) \, dx . \tag{3.3.4}$$

This procedure may be carried out for the function $u(x, t)$ at any instant t, by letting the amplitudes of the modes be functions of t,

$$u(x, t) = \sum_{n=1}^{\infty} \alpha_n(t) \sqrt{2} \sin(n\pi x) . \tag{3.3.5}$$

For small perturbations of the solution $u_e(x, t) = 0$ we may neglect the cubic term in (3.3.1). Decomposition of (3.3.1) in Fourier modes, multiplication by $\sqrt{2} \sin(m\pi x)$ and integration over [0, 1] yields for each m an ordinary differential equation describing the evolution of the amplitude $\alpha_m(t)$

$$\dot{\alpha}_m = (b - m^2\pi^2) \alpha_m \qquad (m = 1, 2, \ldots) . \tag{3.3.6}$$

The result is that for $b < \pi^2$ all amplitudes decay to zero and that as b surpasses the value π^2 the first eigenmode becomes unstable, while all the others remain stable.

Eq. (3.3.1) is called a *reaction–diffusion* equation, because it is an evolution equation for $u(x, t)$ in which there is a reaction part ($bu - u^3$) and a diffusion part ($\partial^2 u / \partial x^2$). Note that the diffusion enhances the stability compared with the pure reaction equation ($\dot{u} = bu - u^3$), which loses stability for the 'null' solution as b becomes larger than zero (cf. eq. (3.1.1)).

I will calculate now what happens when b is slightly larger than π^2. Therefore I introduce the parameter

$$\delta = b - \pi^2 . \tag{3.3.7}$$

Since it is the first eigenmode that becomes unstable one expects a bifurcating solution – supposing one exists – to be dominated by this mode. However, the solution cannot consist solely of this mode as may be verified by inserting the trial solution $u_e(x) = \varepsilon \sin(\pi x)$ in (3.3.2). With the choice $\varepsilon = 2\sqrt{\delta/3}$ the remaining terms are of order ε^3 and this suggests a series expansion.

I shall call the static amplitude of the first mode ε. It is defined by

$$\varepsilon = \int_0^1 u_e(x) \sqrt{2} \sin(\pi x) \, dx \tag{3.3.8}$$

and I try to find an expression for the static solution in terms of

$$u_e(x) = \sum_{n=1}^{\infty} \frac{\varepsilon^n}{n!} u_n(x) \tag{3.3.9}$$

with $u_n(x)$ an arbitrary function and

$$\delta(\varepsilon) = \sum_{n=1}^{\infty} \frac{\varepsilon^n}{n!} a_n \tag{3.3.10}$$

with the a_n denoting the coefficients in this series expansion. Inserting these expressions in the evolution equation and collecting the terms for equal exponents of ε we have to the third order in ε

$$\varepsilon \frac{\partial^2 u_1}{\partial x^2} + \varepsilon \pi^2 u_1 = 0 \tag{3.3.11}$$

$$\frac{\varepsilon^2}{2} \frac{\partial^2 u_2}{\partial x^2} + \frac{\pi^2 \varepsilon^2 u_2}{2} + \varepsilon^2 a_1 u_1 = 0 \tag{3.3.12}$$

$$\frac{\varepsilon^3}{6} \frac{\partial^2 u_3}{\partial x^2} + \frac{\pi^2 \varepsilon^3 u_3}{6} + \frac{\varepsilon^3 a_1 u_2}{2} + \frac{\varepsilon^3 a_2 u_1}{2} - \varepsilon^3 u_1^3 = 0 . \tag{3.3.13}$$

The solution of (3.3.11) is $u_1(x) = c_1 \sqrt{2} \sin(\pi x)$ with c_1 an arbitrary constant. The definition of ε in (3.3.8) implies $c_1 = 1$ and

$$\int_0^1 u_n(x) \sqrt{2} \sin(\pi x)\, dx = 0 \qquad \text{for } n \geq 2 . \tag{3.3.14}$$

This means that none of the functions u_n for $n \geq 2$ have components along the first eigenmode. Applying this to (3.3.12) gives $a_1 = 0$. The solution of (3.3.12) yields $u_2(x) = c_2 \sqrt{2} \sin(\pi x)$, but the normalization condition (3.3.14) only allows $c_2 = 0$. Because $u_3(x)$ has no component along the first eigenmode either, integration of (3.3.13) over [0, 1] after multiplication with $\sqrt{2} \sin(\pi x)$ yields

$$a_2 = 3 \tag{3.3.15}$$

and the resulting equation for u_3 is

$$\partial^2 u_3 / \partial x^2 + \pi^2 u_3 = 12 \sqrt{2} \sin^3(\pi x) - 9 \sqrt{2} \sin \pi x . \tag{3.3.16}$$

I use the goniometrical identity

$$\sin^3(\pi x) = \tfrac{3}{4} \sin(\pi x) - \tfrac{1}{4} \sin(3 \pi x) \tag{3.3.17}$$

which is easily derived from the definition of the sine function

$$\sin(\pi x) = (e^{i\pi x} - e^{-i\pi x})/2i \tag{3.3.18}$$

to find the simplified expression

$$\partial^2 u_3/\partial x^2 + \pi^2 u_3 = -3\sqrt{2}\sin(3\pi x)\,. \tag{3.3.19}$$

The solution is

$$u_3(x) = \frac{3\sqrt{2}}{8\pi^2}\sin(3\pi x)\,. \tag{3.3.20}$$

Thus

$$\delta = \tfrac{3}{2}\varepsilon^2 + O(\varepsilon^3) \tag{3.3.21}$$

$$u_e(x) = \varepsilon\sqrt{2}\sin(\pi x) + \frac{\varepsilon^3\sqrt{2}}{16\pi^2}\sin(3\pi x) + O(\varepsilon^4)\,. \tag{3.3.22}$$

It can be shown that the cubic term in (3.3.21) and the quartic term in (3.3.22) are zero.

I return now to the original variables and express $u_e(x)$ as a series in $(b - \pi^2)$. This may be accomplished by successive substitution; that is, I try to find $\varepsilon(\delta)$ as a series in δ. The result is

$$u_e(x) = \pm 2\sqrt{\frac{(b-\pi^2)}{3}}\sin(\pi x) + c_3(b-\pi^2)^{3/2}\sin(3\pi x) + O(b-\pi^2)^{5/2}\,. \tag{3.3.23}$$

The coefficient c_3 depends on a_4, which has not been calculated. Its value may alternatively be calculated by direct substitution of (3.3.23) in (3.3.2). The result is

$$c_3 = \frac{\pm 1}{12\sqrt{2}\,\pi^2}\,. \tag{3.3.24}$$

This result shows a supercritical ordinary bifurcation, with its important component along the eigenmode that becomes unstable at the bifurcation point. The bifurcation diagram for the first eigenmode is analogous to that shown in fig. 3.1. It is generally true for bifurcations in more than one dimension that the important part of the bifurcating solution lies along the destabilised eigenmode. In the words of Iooss and Joseph [27]: 'The part of the problem having a zero projection into the null space is like the lively tail of a little dog'.

This example demonstrates an important result: in the neighbourhood of bifurcation points the problem of solving partial differential equations may be reduced to solving a set of ordinary differential equations. This gives an enormous simplification of the problem and bifurcation theory is therefore very powerful in dealing with partial differential equations.

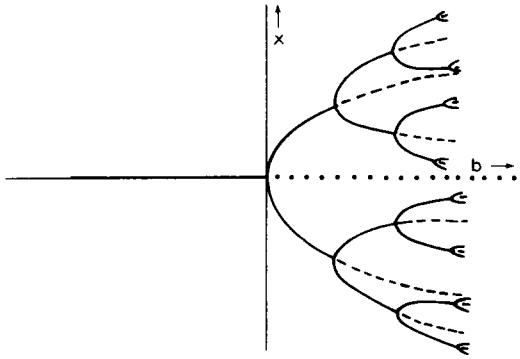

Fig. 3.14. A sketch of a 'tree' of bifurcating solutions.

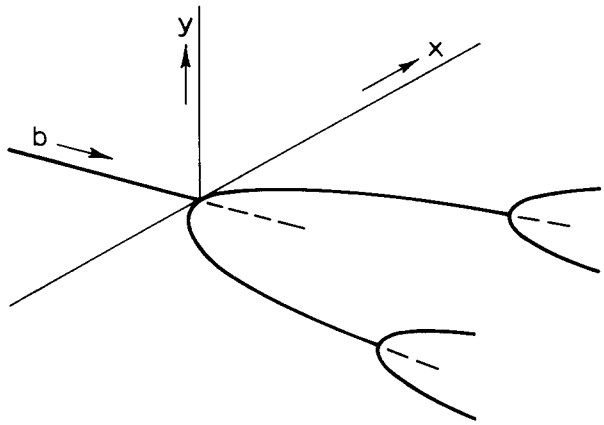

Fig. 3.15. A tree of bifurcations for a partial differential equation. Each successive bifurcation destabilizes a new eigenmode, and increases the dimensionality of the configuration space by one.

All types of bifurcations can occur in partial differential equations including the Hopf bifurcations of the previous section. The stability of the bifurcating branches may again be investigated with the use of small perturbations. For the example above the result is that the branching solutions are stable. As one follows the bifurcated solutions for increasing forcing parameter $-b$ in all our examples – new bifurcations may occur when the bifurcated branch loses stability at some point. Whole 'trees' of bifurcating solutions such as the one sketched in fig. 3.14 for an ordinary differential equation, may be found. For partial differential equations each successive bifurcation may lead to the emergence of a mode that had zero amplitude before. This is illustrated in the three-dimensional drawing, fig. 3.15, for the first two modes. Further bifurcations lead to branches in the 3th and higher dimensions of the Hilbert space of this system.

The particular example of this section has been solved with the use of the method of power series expansion, see [27]. In the literature reference is found to two other methods, the 'Liapunov–Schmidt' method, e.g. Vainberg and Trenogin [34], and the 'centre-manifold' method, see Carr [35]. These methods are mathematically more sophisticated, but series expansion is the most useful in actual computations.

Bifurcation theory has been applied with success in the equations that describe the Rayleigh–Bénard problem, the Taylor experiment, Couette flow and other, related hydrodynamical problems, all described in [33].

3.4. Applications in astronomy

A rough model used to study the dynamical evolution of self-gravitating and rotating gas clouds into rotating single stars or binaries is that of a uniformly rotating self-gravitating fluid whose bounding surface is an ellipsoid. Obviously the fluid assumption of constant density is very unrealistic for stars who are centrally condensed, but it is nevertheless expected that the evolution of these objects bears some qualitative resemblance to the evolution of real stars. The assumption of ellipsoidal surfaces is equally unjustified but is at least more credible.

The great advantage of using both assumptions is that an analytical expression for the gravitational potential can be derived. In the terminology of the introduction this model for dynamical stellar

evolution is 'ad hoc'. Lebovitz [36] has given an extensive review on the theory of binary evolution developed along these lines. Here I shall outline some salient results.

The general expression for the gravitational potential is

$$P(\boldsymbol{r}, t) = -G \int_{V} \frac{\rho(\boldsymbol{r}', t)\, \mathrm{d}\boldsymbol{r}'}{|\boldsymbol{r} - \boldsymbol{r}'|} \tag{3.4.1}$$

where G is the gravitational constant and ρ the density. The integral is taken over the whole fluid volume V. For constant density, ellipsoidal surfaces and a corotating frame the following expression results

$$P(x_1, x_2, x_3) = -\pi G\rho \left\{ I - \sum_{k=1}^{3} A_k x_k^2 \right\} \tag{3.4.2}$$

for points *inside* the fluid surface. Here the axes of x_1, x_2 and x_3 align with the principal axes of the ellipsoid and the coefficients I and A_k are known functions of the semi-axes a_k.

The simplest figure of equilibrium in a rotating frame of reference is an oblate spheroid ($a_1 = a_2 \geq a_3$) as was already shown in 1742 by Maclaurin. In 1834 Jacobi [28] discovered a new set of equilibria with three unequal axes that branches-off from the Maclaurin spheroids as $a_3/a_1 \downarrow 0.583$.

Poincaré in 1885 [29] subsequently described a scenario for stellar dynamical evolution along a path of these equilibria. It is assumed that the density of a Maclaurin spheroid of originally small eccentricity increases slowly, while its total mass and its total angular momentum are preserved. The 'star' becomes more and more oblate until the bifurcation point is reached. In 1883 Thomson and Tait [37] had already shown that for the same mass, density and angular momentum the Jacobi ellipsoid has a lower energy than the corresponding Maclaurin ellipsoid and therefore they expected that the dissipation of energy through viscosity – if on a sufficiently short time scale – would force the star to follow the Jacobi branch.

Further contraction makes the elongation of the Jacobi branch increase until the sequence becomes unstable. Poincaré conjectured that a new pear-shaped equilibrium figure would bifurcate and that still further contraction would make the constricted middle part of the 'pear' grow narrower until finally a pair of orbiting masses would bifurcate: a 'binary system'.

However, stability calculations by Lyapunov in 1905 [38] and Jeans in 1929 [39] have shown that Poincaré's 'pear'-shaped figure is unstable, which puts an end to the Poincaré scenario at the bifurcation point of the Jacobi sequence. Jeans also point out that the 'pear-figure' bifurcation might be subcritical – in the terminology of this review – and that consequently the transition to the binary state would be catastrophical, analogous to the situation in fig. 3.8, described by eq. (3.1.6).

A serious drawback for this 'fission' theory for the origin of binaries is that for classical viscosity coefficients the viscous time scale is orders of magnitude larger than the contraction time scale (Lynden-Bell, 1964 [40]), which implies that the evolution in the neighbourhood of the bifurcation point of the Maclaurin spheroids is not described correctly. Lebovitz (1972, [41]) has reformulated fission theory to account for the practical absence of dissipation. His results outline an evolution along a different path but with qualitatively the same features, first a supercritical and then (possibly) a subcritical bifurcation, see fig. 3.16.

Recently Wiegandt (1981, [42]) has found a point of bifurcation in the sequence of equilibrium configurations of rotating stellar systems, analogous to the Jacobi bifurcation in self-gravitating fluids.

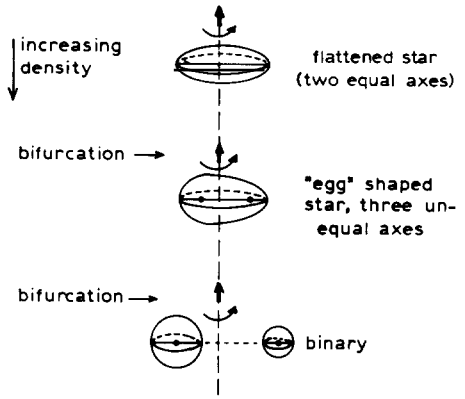

Fig. 3.16. An illustration of the 'fission' theory for the origin of binaries. During the evolution the angular momentum is conserved, while the density increases through contraction.

Again systems with ellipsoidal geometry are assumed and at the bifurcation point a set of three axial equilibria branches-off from the set of axisymmetric equilibria. The analogy with the results above goes so far that exactly the same equations are found.

A bifurcation in the dynamo equations, which describe the oscillating solar magnetic field, is found by Yoshimura [43]. He proves that a steady solution branches-off from the well-known periodic solutions and he suggests that the magnetic fields of the earth and planets and the fields of magnetic stars can be understood this way. In this static solution the dynamo action is everywhere exactly balanced by diffusion so that all time derivatives vanish. The resulting magnetic field configuration is that of a helical tube in the deep part of the dynamo zone.

Relaxation oscillations with limit cycles resulting from Hopf bifurcations have been found in various astrophysical problems. The best-known example is the radial oscillation of variable stars: Cepheids, RR-Lyrae and Mira stars. A description in terms of bifurcation theory can be made by considering the position of the star in the Hertzsprung–Russel diagram as the 'forcing' parameter. For most values of the mass and age of a star – corresponding to a point on the diagram – a static hydrodynamic and thermal equilibrium exists for the atmosphere of the whole star and this equilibrium is attracting (i.e. fluctuations die out). However, at certain values of the forcing parameters the static equilibrium ceases to exist and a cyclic solution branches-off in a Hopf bifurcation. Relaxation oscillations of stars has become a whole separate field in astrophysics, too large to be described in full content here. For an extensive review, see Cox [44].

Thermal limit cycles have been used to explain X-ray burst sources by Barranco et al. [45]. With a simple two-zone model the authors find that helium burning in the envelopes of accreting neutron stars will proceed periodically giving rise to outbursts of X-rays during the relaxation phase phase of the oscillation. Analogous results are suggested by Kuijpers and Pringle [46] for the accretion on white dwarfs.

Recently another thermal relaxation oscillation in the coronae of early type stars has been proposed by Hearn, Kuin and Martens [47]. Hearn and Vardavas in earlier papers [48, 49] had obtained a number of stationary models for stellar coronae using a new method for solving the governing equations of motion, continuity, energy and state. The boundary conditions for this calculation were posed for the first time in a physically meaningful way, namely at two points, one deep in the photosphere of the star were the physical variables are unaltered by the existence of a corona and the other at infinity, where

the gas pressure must vanish. For a given coronal heating mechanism – in this case heating by sawtooth acoustic waves with a given period – the method gives a unique solution to the equations. For a star with a given mass, effective temperature and radius the only remaining input parameter to the equations is the acoustic flux entering at the photospheric boundary. For small values of this parameter Hearn and Vardavas recovered the well-known solution in the form of a stationary, extended, hot corona with supersonic outflow in analogy with the well-known Parker solution for the solar corona (Parker [50]). Further Hearn and Vardavas found that the larger the acoustic flux, the larger the base pressure of the extended corona.

As the acoustic flux – and therefore also the coronal base pressure – surpasses a certain threshold value the extended stationary solution ceases to exist and no other stationary solution can be found. This upper limit for the base pressure of stationary extended coronae had been predicted by Souffrin [51] using rather analytical considerations.

For acoustic fluxes above the threshold Hearn, Kuin and Martens [47] found that the solution to the equations underwent a relaxation oscillation. Although the computer program was not designed to solve the full time dependent set of equations a careful time scale analysis of the dominant physical processes involved showed that the numerical iteration procedure follows the time dependent behaviour. Therefore it is suggested that for large acoustic fluxes – as for example those that heat the coronae of early-type stars – the corona exhibits cyclic behaviour.

Within the context of the present paper this phenomenon can be understood as a subcritical Hopf bifurcation in the set of non-linear partial differential equations that describe the problem. Similar bifurcations are known to take place in the equations that describe analogous hydrodynamical systems, like for example the Rayleigh–Bénard experiment.

The physical mechanism leading to the destruction of the sequence of stationary extended coronae is the well-known radiative instability (Field [52]) that also plays a role in the catastrophes in coronal loops, described in section 2.2. The role of this instability in setting up the relaxation oscillation becomes evident from the following description of the cyclic solution.

As the acoustic flux heating the corona is increased the transition region of the corona moves deeper into the star's chromosphere, while the overall structure of the corona is preserved. During this process the corona is in a quasi-stationary equilibrium, that is; a stationary equilibrium is reached everywhere except at the base of the transition region, on a time scale that is short compared with the time scale for the increase of the base pressure, due to the 'evaporation' process at the base. The heating-up of material increases the total mass of the corona and because the overall temperature structure is conserved the density increases everywhere in the corona. This leads to an increasing energy demand in the outer layers due to increasing stellar wind losses and this energy must be provided by conduction since acoustic heating is negligible there. Consequently the temperature of the outer layers drops somewhat thus steepening the temperature gradient and increasing the conductive flow. As the temperature in the outer layers drops somewhat the energy demand by the stellar wind is also reduced and in principle these two reactions stabilize the stationary solution.

However, as the acoustic flux increases still further the temperature decrease and the density increase in the outer layers increase the importance of radiation losses in the energy budget and as soon as these losses become dominant the radiative instability sets in and the whole outer region of the atmosphere cools down catastrophically. What is left is a thin corona at high pressure with two transition regions, one facing outward and one facing inward. See fig. 3.17 for a sketch of this evolution. Much of the acoustic flux is still dissipated in this thin hydrostatic corona but some of the flux passes through it to form a second corona in the very outer layers of the star. This second corona then moves in again in the

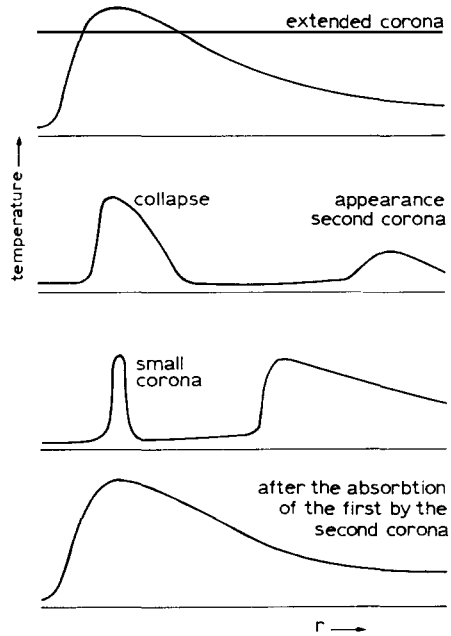

Fig. 3.17. An illustration of the temperature structure of a stellar corona at various phases of the relaxation oscillation. This figure is from Hearn, Kuin and Martens [47].

manner described above until it merges with the thin corona. At this point the original, extended corona is restored, again moves in a bit and finally the outer layers again undergo a radiative collapse.

The description above makes it clear that it is the radiative instability that prevents an extended corona to form at too high pressures while it is the effect of 'evaporation', also described in section 2.2 that makes the transition region move to higher pressure.

A similar cyclic solution was obtained for the plasma in solar coronal loops by Kuin and Martens [53]. The rationale for their model was that the observed vanishing conductive flow at a temperature of about 20 000 K at the base of the transition region in coronal loops (Vernazza et al. [54]) is incompatible with stable static solutions for the thermal structure of hot coronal loops, as was shown in various ways by Antiochos [55], Hood and Priest [56] and Chiuderi et al. [57].

Kuin and Martens described the dominant physical processes in the plasma of coronal loops in an 'ad-hoc' manner, reducing the governing hydrodynamic equations to a set of ordinary differential equations. The results show a cyclic behaviour of the loop plasma with a long lasting 'hot' phase with slowly increasing density followed by catastrophical radiative cooling and draining of the loop. Then the remaining plasma heats up again very quickly and the cycle starts off again. This solution is very similar to that for open coronae, discussed above. The cyclic solution explains the observations of the ceaseless up- and downflows in the solar corona as well as the coexistence of cool and very hot material in coronal loops as is required by the observations of Foukal [58] and Pye et al. [59].

The set of equations solved by Kuin and Martens contains one external parameter (α) which is essentially the ratio of radiative and conductive time scales. The value of this parameter depends (among other things) on the exact slope of the radiative loss function (see fig. 2.4). Kuin and Martens found that for $\alpha > 1$ there is a stable static solution which loses stability as α becomes smaller than unity. At this point a subcritical Hopf bifurcation takes place, so the new solution is an oscillation with

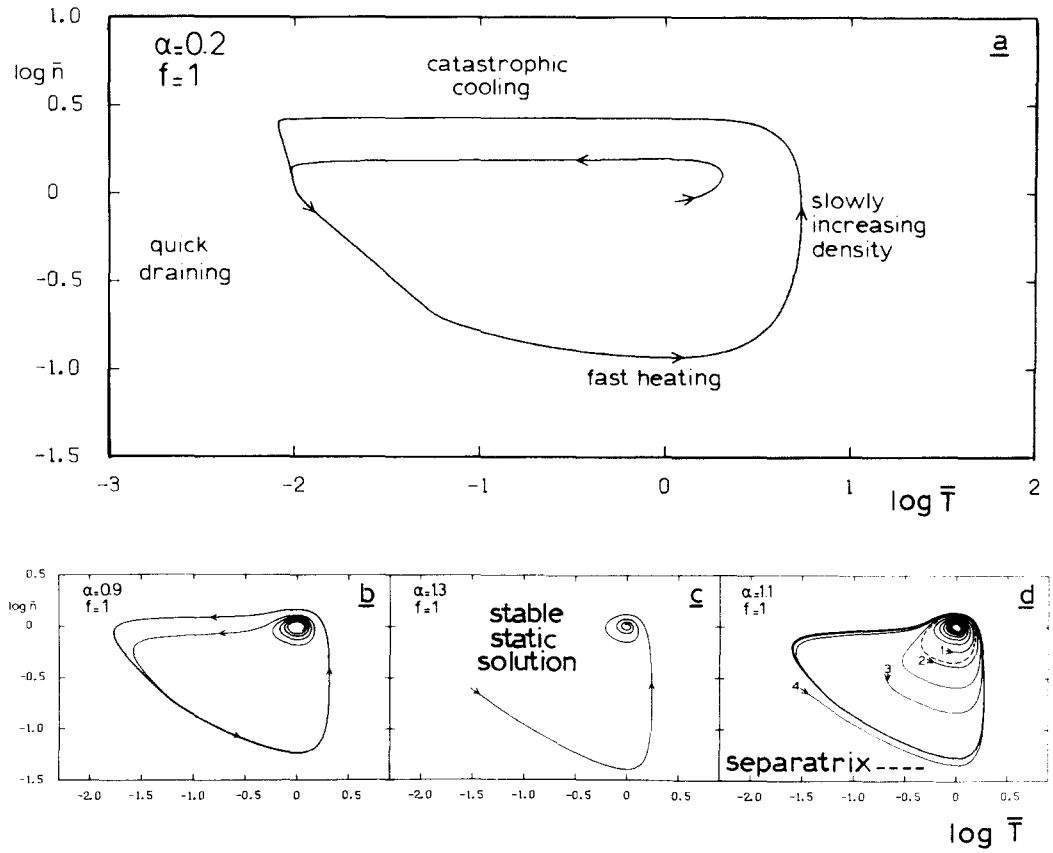

Fig. 3.18. The relaxation oscillation of the plasma in coronal loops in the phase plane of dimensionless temperature versus dimensionless density. At $\alpha = 1.3$ the solution is stable and static. At $\alpha = 1.1$ a stable and static and resp. a cyclic solution coexist while for $\alpha = 0.9$ and $\alpha = 0.2$ only the cyclic solution remains after a subcritical Hopf bifurcation at $\alpha = 1.0$. (For the meaning of α see the text.) This figure is from Kuin and Martens [53].

finite amplitude. For $1 \leq \alpha \leq 1.3$ the coexistence of a stable static solution and a relaxation oscillation was found. In the phase plane of mean plasma density versus mean temperature the 'basin of attraction' of both solutions is divided by a separatrix as is indicated in fig. 3.18. However, for the solar corona the correct value of α is probably around 0.2, so only a cyclic solution is to be expected.

4. The onset of turbulence

4.1. Scenarios for the transition to chaos via bifurcations

A fluid or a gas is said to be turbulent when its behaviour is highly unpredictable. The motion of a test particle in a fluid may be predicted for a certain time ahead, but as time goes on the predictions become less and less accurate. On the other hand turbulent fluids and gases usually have a rather regular *average* behaviour. When $f(\boldsymbol{r}, t)$ is some property of the fluid or gas – like the temperature, pressure or velocity – one expects the limit

$$\bar{f}(\boldsymbol{r}) = \lim_{\tau\to\infty} \frac{1}{\tau} \int_0^\tau f(\boldsymbol{r}, t)\, \mathrm{d}t \tag{4.1.1}$$

to exist and to be independent of $f(\boldsymbol{r}, 0)$, but rather depend on quantities describing the totality of the fluid, like energy content, volume, or on the external forces, like the temperature difference between the boundaries in the Rayleigh–Bénard experiment. (The original experiment, by Bénard, was performed on whale oil, see Bénard, 1901 [60].)

There is a conception of turbulence which goes back to the 1940's and is due to Landau [61] and Hopf [62], and which is worked out in Landau and Lifshitz [63]. It may seem a rather logical generalisation of the bifurcation theory of the last section. It was shown that in Hopf bifurcations an attracting point sheds a limit cycle as the forcing parameter increases and it is straightforward to extend this idea to higher dimensions. In three dimensions a limit cycle may shed an attracting torus, which is a surface in three-dimensional space containing periodic motion with two frequencies whose ratio is not a rational number (if the ratio were rational any particle trajectory on the torus would finally reach a point where it had already been and the trajectory would degenerate into a one-dimensional curve, i.e. a complicated limit cycle). In higher dimensions more and more tori with periodic motions that are rationally independent might shed off and this might continue to infinity. Finally there would be left a motion with uncountably many rationally independent frequencies that gives a Fourier spectrum that cannot be distinguished from the smooth Fourier spectrum obtained in certain experiments on turbulence, for example in the Rayleigh–Bénard experiment at high Rayleigh numbers (Gollub et al. [64]).

This scenario for the transition to chaos via an infinite cascade of bifurcations requires an infinite number of degrees of freedom for the fluid motion, but this is no problem, since the fluid motion is described by *partial* differential equations, which *do* have infinite degrees of freedom (cf. section 3.3). However, there is an intuitive objection against such an idea. Because the turbulent gases and fluids are all viscous and conducting one expects such a thing as a smallest scale for the variation in the fluid variables. For example for the temperature

$$|T/\nabla T| \geq l \tag{4.1.2}$$

where l is some length that is determined by the thermal conductivity. The temperature structure in a fluid with given dimensions would then be described by a finite number of eigenmodes, with length scales in between the largest length in the fluid and l. This finite number of eigenmodes would restrict the phase space of the system to finite dimensions and consequently only a finite number of bifurcating tori would be possible.

A much more serious objection against the Landau and Hopf idea comes from Bass [65], who called attention to the fact that multiperiodic solutions unlike turbulent solutions, do not phase mix. The experiments on turbulence show that the autocorrelation function $g(\tau)$

$$g(\tau) = \lim_{\tau\to\infty} \frac{1}{\tau} \int_0^\tau f(t + t_0) f(t)\, \mathrm{d}t \tag{4.1.3}$$

decays to zero as $t_0 \to \infty$. This is not true for the multiperiodic functions in the Landau–Hopf scenario, see Joseph in [66].

It was realised by Ruelle and Takens, in a now celebrated paper [67], that turbulence is a phenomenon that will already occur after a few bifurcations. Unlike in the Landau–Hopf idea turbulence is not connected with *periodic* attractors, such as limit cycles or tori, but with a new type of attractor: the *strange* attractor. The Ruelle–Takens idea of turbulence is in agreement with the intuitive idea mentioned above that turbulence must be explained as a finite dimensional phenomenon.

4.2. Chaos in one-dimensional maps

The first-order difference equation to be studied here comes from ecology and describes a seasonally breading population in which generations do not overlap (May, in "Theoretical Ecology" [68] and in a review paper [69]). The population in the $(n+1)$th season is proportional to the number x_{n+1} and it depends on the population in the former season as

$$x_{n+1} = bx_n(1 - x_n)\,. \tag{4.2.1}$$

This equation describes the tendency of the population to increase from one generation to the next when it is small ($x_n \ll 1$) and for it to decrease when it is large (e.g. by food shortage). It comes back in many contexts, see review [69] and references therein.

b will be restricted here to $0 < b < 4$ so that the interval $[0, 1]$ is mapped onto itself. Only initial values in this domain will be considered so that any sequence of x will remain in it. One of the appealing features of the above equation is that one can study its solutions and verify its strange behaviour as b increases on a simple programmable pocket calculator. For $b < 1$ all solutions decay to zero and for $1 < b < 3$ there is an attracting point solution that is not zero. There is a nice graphical way to study the solutions of eq. (4.2.1) (e.g. Hofstadter [70]) that is displayed in fig. 4.1. The parabola in the figure is the function $bx(1-x)$ and it gives the image x_{n+1} of a certain x_n. After having obtained x_{n+1} one may transform this image into a new original by drawing a horizontal curve that intersects the line $x_{n+1} = x_n$ at some point. From that point the procedure can be repeated as is demonstrated in fig. 4.1. For $b < 1$ all solutions converge to $x = 0$. For $b > 1$ the stable attracting solution is located at the intersection of the line and the parabola, the other point that is mapped into itself.

A very elegant way to study the stability of the solutions is described by May [69], to which we refer

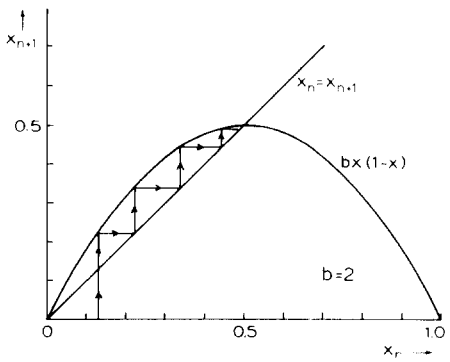

Fig. 4.1. A stable point solution of eq. (4.2.1).

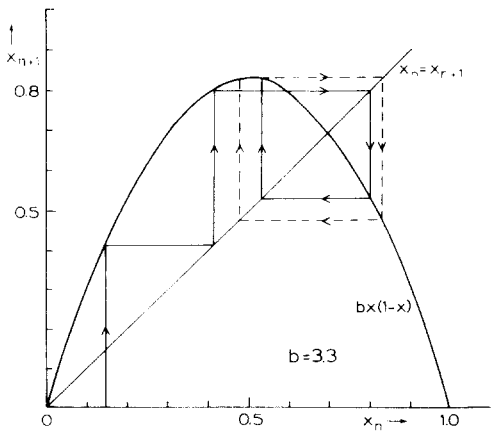

Fig. 4.2. A period 2 solution of eq. (4.2.1).

the interested reader. It is found that as b becomes larger than 3 the static solution loses its stability and gives way to a periodic solution with period 2. This solution is displayed in fig. 4.2. There is a clear analogy here of course with the Hopf bifurcation in differential equations.

At $b = 3.45$ a new bifurcation occurs and now an attracting periodic solution with period 4 originates. As b is increased further the behaviour becomes more and more complicated. Cycles with higher and higher periods – always 2^n – bifurcate, but the parameter 'window' – in b – for each cycle becomes increasingly shorter. There is a point of accumulation in the domain of b for this succession of bifurcations at $b = 3.5700\ldots$. Beyond that value all cycles of period 2^n are passed and the behaviour of x becomes "chaotic", see fig. 4.3. We need to be more precise about this chaotic behaviour. It is characterised by two phenomena:

1. Sensitivity to initial data. Two sequences x_n, x_{n+1}, etc. with slightly different initial values become totally different after a finite number of iterations. This means that the long term behaviour of the system is essentially unpredictable: no matter how precise the initial values are, in the long run this will not be precise enough.

2. Aperiodicity. There is an uncountable subset of initial data which never set down to periodic behaviour. The Fourier plot of these sequences is smooth, just as in some experiments on turbulence. There are also uncountably many initial data which lead to stable periodic orbits, as was shown by Li and Yorke [71]. It is proven by Guckenheimer [72] that there is one 'stable' cycle for each value of b that attracts almost all orbits. However, this cyclic behaviour is *completely* destroyed by small arbitrary disturbances. Yorke and Yorke [73] investigated the slightly noisy equation

$$x_{n+1} = 3.83x_n(1 - x_n) \pm 0.001 \tag{4.2.2}$$

where the sign of 0.001 is chosen randomly at each iteration. It was found that periodicity completely disappeared. Note that for $b < 3.5700\ldots$ this noise would *not* destroy the stability. There would be fluctuations around the static solution or around the stable periodic orbits of the order of 0.001. Further it is noted that even without the noise it takes thousands and thousands of iterations before the transients associated with the initial conditions are damped out and periodicity sets in. Therefore, for all practical purposes the solutions are chaotic.

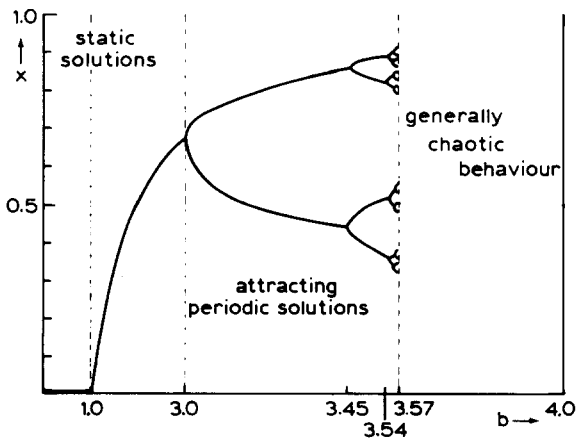

Fig. 4.3. The sequence of static, periodic and chaotic behaviour as b increases in eq. (4.2.1). Note the changes in scale at $b = 3.0$ and at $b = 3.5700$.

These solutions demonstrate chaos in a system with one degree of freedom, although it was not described by a differential equation, but by a difference equation. It will be demonstrated in the next section that there is a close connection between difference equations and differential equations in higher dimensions, via the method of Poincaré sections. This one-dimensional model already shows chaotic behaviour, in complete contrast with the Landau and Hopf picture, which involved infinitely many degrees of freedom. It should be noted that this example is also in contrast with the Ruelle–Takens picture, who claimed that the onset of chaos already occurs after a few bifurcations, while for eq. (4.4) there are infinitely many bifurcations before chaos sets in.

This behaviour need not be characteristic for the onset of chaos. In the next section there is an example of the coexistence of chaos and periodic solutions after only a few bifurcations. The Fourier spectrum of such a system gives a few peaks at the frequencies of the cyclic solutions and a 'noisy' background, due to the chaotic behaviour. May [69] also gives some examples of direct transition from point attractors to chaos in one-dimensional mappings ($x_{n+1} = f(x_n)$).

In the region $3 < b < 3.5700\ldots$ of the example (4.2.1) an attracting 2^n-period orbit sheds of a 2^{n+1}-period orbit as b increases. These bifurcations occur after smaller and smaller intervals in b, until convergence is reached at $b = 3.5700\ldots$. Feigenbaum [74] discovered on a simple calculator that these 'windows' of periodicity converge at a universal rate. Let b_n be the value of b at which a cycle of period 2^n is shed off. Then the ratio of two succeeding intervals is more and more accurately described by

$$\left| \frac{b_n - b_{n-1}}{b_{n+1} - b_n} \right| = \delta = 4.669\ldots \tag{4.2.3}$$

as n increases. Using this expression one may derive

$$b_n \simeq b_\infty - c\delta^{-n}. \tag{4.2.4}$$

In the mapping of eq. (4.2.1) $c = 2.661\ldots$ and $b_\infty = 3.5700\ldots$. This Feigenbaum sequence has turned out to be a universal sequence for the period doubling bifurcations in all sorts of problems! b_∞ and c are dependent on the problem one is concerned with but δ is a universal constant for dissipative mappings – i.e. difference equations, with the absolute value of the Jacobian smaller than unity, that are consequently area contracting. Many Feigenbaum sequences have been discovered numerically and experimentally. References to a whole forest of Feigenbäume in all sorts of situations are given in [75].

An important conclusion that has been made in the study of Feigenbaum sequences is that full – i.e. large scale – chaos sets in beyond the point of convergence of the sequence. Thus one may predict large scale chaos knowing only the values of the forcing parameters belonging to the first two periodic bifurcations: given the values of δ (a universal constant), b_1 and b_2 (problem dependent), b_∞ can easily be calculated with eq. (4.2.4).

4.3. Strange attractors and turbulence

Turbulence is a phenomenon that is encountered in dissipative fluids and gases under strong external forcing. When the forcing is stopped all motion finally damps out and the system settles down in its rest state. Under moderate external forcing the system settles down in a steady state: for example convective cells in the Rayleigh–Bénard experiment. This settling down is an example of *insensitivity to initial data*. It does not matter at which state the system is in the beginning of the experiment, its final

state is always the same. Sometimes the situation is slightly more complicated because there is more than one final state for a given forcing and each final state *attracts* a whole set of initial states. Within such a set insensitivity to initial data remains however.

Attractors are mathematical objects that may describe such situations. In sections 2 and 3 there are many examples of point- and periodic attractors. These attractors exhibit insensitivity to initial data just as dissipative fluids. Static solutions that are unstable – all the dotted curves in section 2 – are called 'repellors' or 'separatrices'. These objects show *sensitivity to initial data.* Two points separated by a separatrix, no matter how small their initial distances, always end up at a finite distance in the phase space – and in real space! Turbulence is an example of a phenomenon that is highly sensitive to initial data, but the situation in turbulent fluids is much more complicated than the examples in section 2, in which there is always a finite number of separatrices. Two points at an infinitesimal distance, but further located arbitrarily in the phase space are unlikely to be separated by a separatrix. In turbulent fluids, however, *any* two randomly chosen sets of initial data diverge as time goes on. Does that mean that there is an infinite number of generalised separatrices?

On the other hand it seems that not all possible states are realised in a turbulent fluid. On the average turbulent fluids look "alike", whatever the initial conditions might have been. Hence the system probably still has some attracting properties and should be described by an attractor. Moreover, the fluid has recognizable attracting states for all situations except turbulence and these attracting states are essentially connected with dissipation, so it would seem reasonable to expect some attractor being related with turbulence.

Thus, what one is looking for, is some mathematical object to account for turbulence, which is an attractor but at the same time exhibits sensitivity to initial data and thereby is a repellor.

That such an object might exist can be made plausible by an analogy with an object of the "real" world: the labyrinth. People who get into a labyrinth never come out – if it is a good labyrinth – and thereby the labyrinth resembles an attractor. On the other hand, once inside, the path of each person becomes highly chaotic and two persons entering through the same gate might follow completely different pathways. In the long run each person will visit almost every point in the labyrinth, so some must be able to get out (we note that also in strange attractors some, but only very few, orbits can leave the attractor, see Rabinovitch [76]). The distribution of many persons in the labyrinth will be a nice smooth function after some time, even when they all started at the same place at the same time.

The first strange attractor in the literature comes from the field of meteorology and was discovered in 1963 by Lorenz [77] in a pioneering paper on non-static non-periodic solutions. The Lorenz system was based on equations introduced by Saltzmann [78] who was investigating convection in the earth's atmosphere. The derivation of the Lorenz equations is a nice example of the way 'ad hoc' equations originate in the practice of research and therefore the derivation will be repeated in some detail here.

Saltzmann approximated the atmosphere as a fluid of uniform depth H and with a temperature difference ΔT between upper and lower boundary. The horizontal extent of the fluid is assumed to be much larger than H and further it is assumed that all motions are parallel to the x,z-plane and that no variations along the y-axis occur. Gravity is directed along the z-axis. These assumptions combined with the fluid assumption of constant density imply that the fluid velocity may be derived from a stream function

$$V_x = \partial\psi/\partial z\ ; \qquad V_z = -\partial\psi/\partial x\,. \tag{4.3.1}$$

Note, however, that strict application of the assumption of constant density would eliminate the

possibility of convection, for convection is based on the Archimedes force due to the density differences between cool and hot bubbles of a fluid. In the Oberbeck–Boussinesq approximations the temperature dependence of the density is taken into account in the gravity term only and thus the theoretical advantage of the constant density assumption is retained. This approximation was derived by Spiegel and Veronis in 1960 to study stellar convection [79] (see also Busse [32] for a discussion and further references). Using the stream function and the Oberbeck–Boussinesq approximation, Saltzmann reduced the governing hydrodynamical equations to the form

$$\frac{\partial}{\partial t}\nabla^2\psi = -\frac{\partial(\psi, \nabla^2\psi)}{\partial(x, z)} + \nu\nabla^4\psi + g\alpha\frac{\partial\theta}{\partial x}$$

$$\frac{\partial}{\partial t}\theta = -\frac{\partial(\psi, \theta)}{\partial(x, z)} + \frac{\Delta T}{H}\frac{\partial\psi}{\partial x} + \kappa\nabla^2\theta\,. \tag{4.3.2}$$

Here the first terms on the right hand sides are Jacobians

$$\frac{\partial(\psi, \theta)}{\partial(x, z)} = \frac{\partial\psi}{\partial x}\frac{\partial\theta}{\partial z} - \frac{\partial\psi}{\partial z}\frac{\partial\theta}{\partial x} \tag{4.3.3}$$

and θ is the departure of the temperature from that in the static state, in which the energy is transferred through conduction. The constants g, α, ν and κ denote respectively the acceleration of gravity, the coefficient of thermal expansion, the kinematic viscosity and the thermal conductivity. ψ and $\nabla^2\psi$ are assumed to vanish at both boundaries.

The eqs. (4.3.2) have a steady state solution $\theta = \psi = 0$ that becomes unstable as the Rayleigh number

$$R = g\alpha H^3\,\Delta T/\nu\kappa \tag{4.3.4}$$

exceeds the critical value

$$R_c = \pi^4(1 + a^2)^3/a^2\,. \tag{4.3.5}$$

As R surpasses this value convection sets in. The coefficient a in R_c determines the "flatness" of the convective rolls that originate. When $a^2 = \frac{1}{2}$, R_c reaches its minimum value, 657.51.

Saltzmann replaced the partial differential eqs. (4.3.2) by an infinite set of ordinary differential equations by expressing ψ and θ as Fourier series in x and z with the coefficients as functions of t alone. (A completely analogous procedure has been followed in the example of section 3.3.) The non-linear terms containing products of trigonometric functions were replaced by sums of trigonometric functions and this made it possible to equate the coefficients of the Fourier terms separately. Lorenz in his paper made the drastic approach of considering only the following terms

$$\frac{a}{1 + a^2}\frac{\psi}{\kappa} = X\sqrt{2}\sin(\pi ax/H)\sin(\pi z/H)$$

$$\pi\frac{R_a}{R_c}\frac{\theta}{\Delta T} = Y\sqrt{2}\cos(\pi ax/H)\sin(\pi z/H) - Z\sin(2\pi z/H)\,. \tag{4.3.6}$$

Thus $X(t)$ represents the convective overturning, and $Y(t)$ and $Z(t)$ represent respectively the horizontal and vertical temperature variations. These expressions are substituted in eqs. (4.3.2) and all the other Fourier components than those in the expressions above are ignored. The resulting expressions are so-called 'truncated mode' equations:

$$\begin{aligned} \dot{X} &= -\sigma X + \sigma Y \\ \dot{Y} &= bX - Y - XZ \\ \dot{Z} &= XY - \alpha Z . \end{aligned} \tag{4.3.7}$$

The dimensionless time is

$$\tau = \pi^2(1 + a^2)\kappa t/H^2 \tag{4.3.8}$$

and the dot denotes differentiation with respect to τ. $\sigma = \nu/\kappa$ is the Prandtl number, $\alpha = 4/(1 + a^2)$ and the forcing parameter represents the Rayleigh number: $b = R/R_c$. In the following I will use the parameter values $\sigma = 10$ and $\alpha = 8/3$, corresponding with $a^2 = \frac{1}{2}$. It can be shown that the neglect of all but three Fourier components is incorrect for large values of the Rayleigh number R, see McLaughlin and Martin [80], but the Lorenz equations have nevertheless become a sort of 'Rosetta stone' in the rapidly expanding field of strange attractors and turbulence. The equations show up in the description of a number of physical systems, also in astrophysics (see section 4.5). For a short description and reference to physical models leading to the Lorenz equations, see Yorke and Yorke [73]. Sparrow [81] has recently written an extensive and transparant book dedicated solely to the Lorenz equations, from a mathematical point of view. He also treats solutions for other values of the parameters σ and α than the usual ones.

The model eqs. (4.3.7) are again very simple, contain a forcing parameter, and can easily be solved numerically. The system is truly dissipative in the sense that its volume in phase space shrinks continuously. The expansion rate of a volume element $\delta V = \delta X\, \delta Y\, \delta Z$ in phase space is given by

$$\frac{1}{\delta V}\frac{\mathrm{d}}{\mathrm{d}t}(\delta V) = \frac{\partial \dot{X}}{\partial X} + \frac{\partial \dot{Y}}{\partial Y} + \frac{\partial \dot{Z}}{\partial Z} = -(\alpha + 1 + \sigma) < 0 . \tag{4.3.9}$$

Yet the solutions do not settle down to a static or periodic state. An example of a solution for $b = 28$ and the origin as initial value is given in fig. 4.4. The non-periodicity of this solution is reflected in fig. 4.5 which shows the Fourier spectrum of $X(t)$: the spectrum is clearly smooth. Sensitivity to initial data is shown in fig. 4.6. The position of a large set of points is projected into a plane. These points had started very close together (within the resolution of the figure) 27.7 time units of eqs. (4.3.7) earlier but in the figure they fill the whole space of this 'butterfly' attractor. The non-periodicity and sensitivity to initial data cause all the time dependent correlation functions between variables to decay to zero as $t \to \infty$, just as in the experiments on turbulence.

As in the preceding examples of this review there is a tunable parameter b in the Lorenz equations that determines the nature of the solutions. It is easily verified that for $b < 1$ the origin is an attractor. At $b = 1$ a bifurcation occurs and two additional static solutions develop. When b becomes larger than 24.74 no stable static solution remains and the solution is chaotic, such as in the example that has been given for $b = 28$. In the region $24.06 < b < 24.71$ there seems to be an analogon of the subcritical Hopf

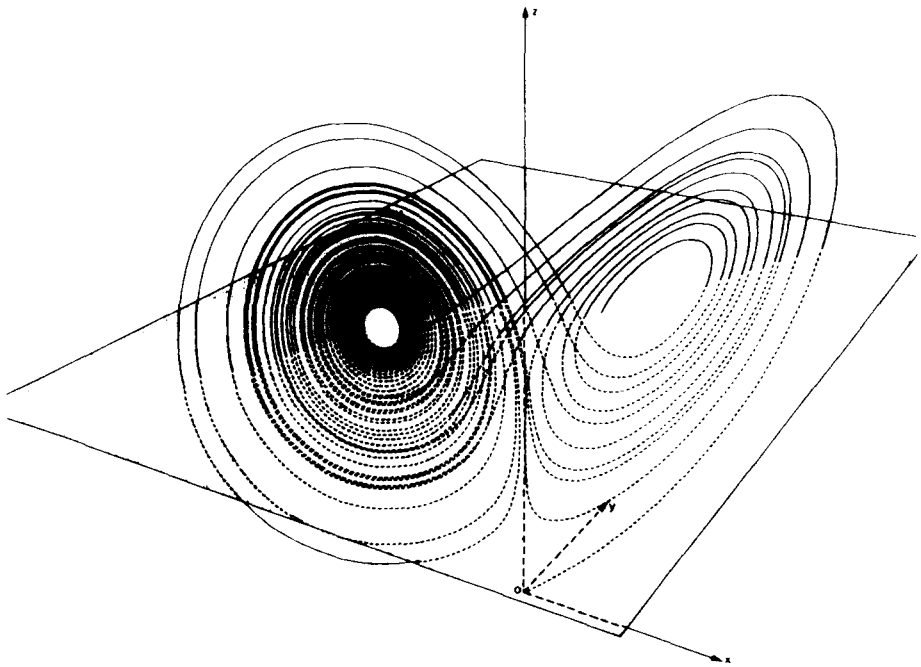

Fig. 4.4. A perspective view of a solution of the Lorenz equations (4.3.7) with $b = 28$, $\sigma = 10$ and $\alpha = 8/3$. This figure is from Ruelle [115]. Courtesy of la Récherche and D. Ruelle.

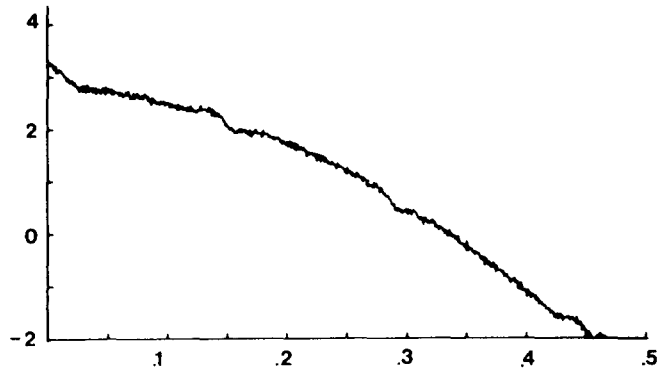

Fig. 4.5. The Fourier spectrum of the variable $X(t)$ in a solution of the Lorenz equations with the same parameter values as in fig. 4.5.

bifurcation. In this parameter range there are two stable static solutions – point attractors – coexisting with solutions that oscillate irregularly forever. Each solution has its 'basin of attraction', that is a region in phase space in which all orbits are attracted.

In autonomous differential equations – i.e. equations without explicit time dependence – strange attractors appear first when there are three degrees of freedom, just as the periodic attractor originates in two dimensions. At present it is impossible to tell whether there will be yet other types of attractors in higher dimensions. That three dimensions is the absolute minimum for a strange attractor follows from the Poincaré–Bendixson theorem [83], which states that for two degrees of freedom the only

Fig. 4.6. The projection into a plane of the positions of 3072 points at $t = 27.7$ (in the units of eq. (4.3.8)) that all had started at the same point within the resolution of this figure at $t = 0$. Figs. 4.5 and 4.6 are from D. Farmer et al. [116]. Courtesy of the New York Academy of Sciences and the authors.

attractors are point attractors and periodic attractors. An overview of the types of attractors discussed in this review is given in table 1.

There are many types of strange attractors in between simple limit cycles and truly chaotic attractors. Many attractors give overall oscillatory solutions which seem to be disturbed by some noise only. Helleman prefers to reserve the word aperiodic attractors for these objects [82]. Others display as much noise as oscillatory behaviour and some are chaotic with only some reminiscence of periodicity. A continuous transition from periodicity to chaos takes place in the Rössler equations [84] as their tunable parameter is increased,

$$\begin{aligned} \dot{x} &= -y - z \\ \dot{y} &= x + by \\ \dot{z} &= 0.4 + xz - 8.5z\,. \end{aligned} \tag{4.3.10}$$

Figure 4.7 displays the projection of a solution in the x,y-plane together with the Fourier spectra for increasing values of b. This may be compared with the power spectra for the velocity in the

Table 1
Scheme of attractors

Number of independent variables = dimension of phase space	Type of attractor	Type of solution
1	point attractor	stable static equilibrium
2	periodic attractor (and point attractor)	stable oscillation: limit cycle
3	strange attractor (and point attractor plus periodic attractor)	chaos: – sensitivity to initial data – aperiodicity

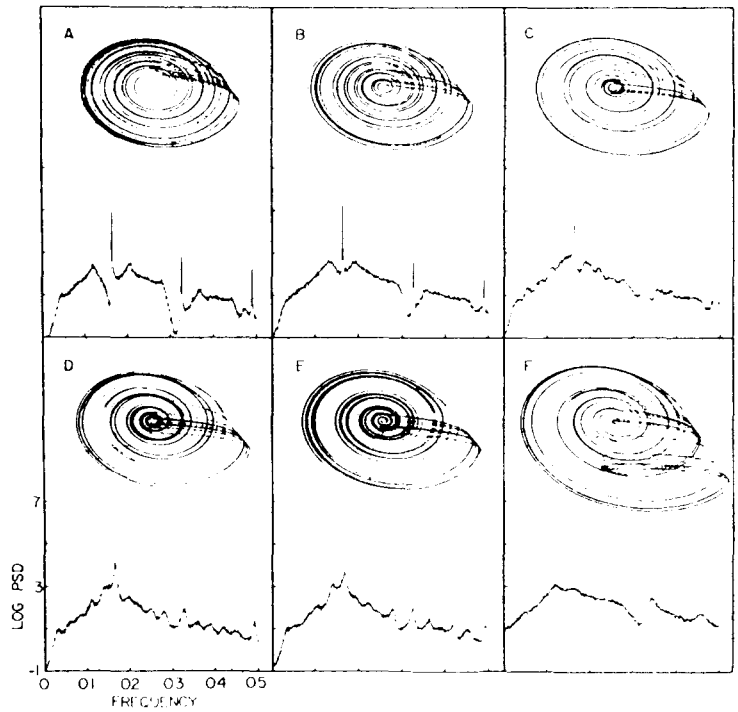

Fig. 4.7. A perspective view of the solutions of the Rössler equations and the corresponding Fourier spectra of the variable $x(t)$. For $b = 0.15$ (A), 0.17 (B), 0.18 (C), 0.19 (D), 0.20 (E), 0.30 (F). From D. Farmer et al. [116]. Courtesy of the New York Academy of Sciences and the authors.

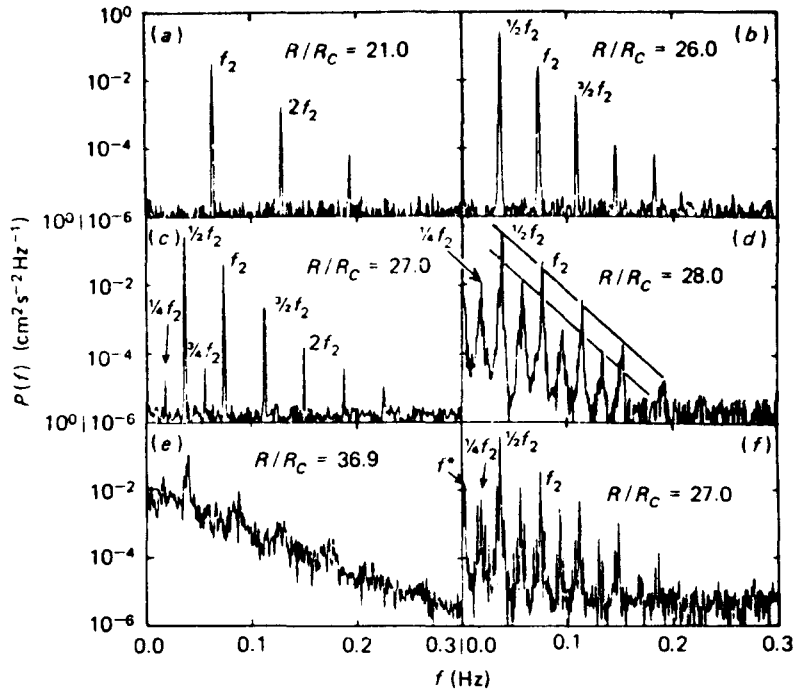

Fig. 4.8. Fourier spectra of the velocity in the Rayleigh–Bénard experiment on water. R is the Rayleigh number. R_c is the Rayleigh number at which the static solution disappears. This figure is from J.P. Gollub, S.V. Benson and J. Steinman [64]. Courtesy of the New York Academy of Sciences and the authors.

Rayleigh–Bénard experiment on water (Gollub et al. [64]), depicted in fig. 4.8. As the Rayleigh number (R) in the fluid increases, more and more periods bifurcate – analogous to the period doubling sequences in the one-dimensional mappings in the previous section – and at the same time the amplitude of the smooth part of the spectrum increases, until full turbulence is reached in fig. 4.8e. Upon lowering the Rayleigh number, fig. 4.8f, to a previous value – that of fig. 4.8c – the old situation is not restored: the spectrum remains 'noisier' than before and a new period f^* has emanated.

The Rössler equations above have no physical relation with the Rayleigh–Bénard experiment and the similarities in the evolution of the Fourier spectra are not more than a mathematical simulacrum. However, it is now generally felt that there is a connection between turbulence and strange attractors and therefore that turbulence is a phenomenon that may already occur in systems with only three degrees of freedom. The route to chaos described above – a sequence of period doubling bifurcations converging at an accumulation point, followed by aperiodic behaviour – is one of the many possible routes to turbulence. Another possibility which is less well supported by experiments is the onset of chaos after only a few bifurcations as in the Ruelle and Takens scenario [67].

An important goal of contemporary research lies in verifying that the properties of strange attractors (sensitivity to initial data and aperiodicity) are indeed properties of the system in study, that are carried over to the truncated mode equations and that despite of the usually drastic approximations these properties are not introduced somewhere in the derivation. In particular the relation between the truncated mode equations and the original partial differential equations is of interest.

The first 'missing link' has recently been found by Moore, Toomre, Knobloch and Weiss [85] in the study of two-dimensional thermosolutal convection in an incompressible fluid. These authors have numerically solved the governing hydrodynamical *partial* differential equations and they clearly reproduced a sequence of period doubling bifurcations followed by chaos.

Moreover, they found great similarity between their solutions and earlier truncated mode solutions of the same system (Knobloch and Weiss [86]) even though it can be shown that the truncated mode equations are not always valid approximations to the partial differential equations.

Now I return to the question of the connection between difference equations and differential equations. Consider the motion of a point in three-dimensional phase space governed by some system of differential equations. The problem may be reduced by considering only the intersection of the trajectory with a given plane in phase space, for example the plane $z = 0$. Each intersection of the plane and the trajectory – if there is one – has coordinates $(x_{n+1}, y_{n+1}, 0)$ and is completely determined by the coordinates of the nth iteration, because the future trajectory of the point in phase space is completely determined when the initial set of coordinates is given. Hence there must exist a transformation

$$x_{n+1} = f(x_n, y_n), \qquad y_{n+1} = g(x_n, y_n) \tag{4.3.11}$$

that contains enough information to decide whether the solution to the original equations is chaotic or regular. These mappings are called Poincaré- or return mappings. The real problem of course is finding the functions f and g and in general this cannot be done. The alternative approach is to *define* a mapping of the type of eq. (4.3.11) and then study directly its properties. The obvious advantage of this approach is that the problem is reduced to one that can be solved on any programmable pocket calculator. The disadvantage is that there is an enormous distance now between the original problem and the difference equations at hand.

The first authors to consider the approach of defining a mapping were Hénon and Heiles in 1964 [87], in a paper that will be discussed in the next section. Hénon [88] also introduced a mapping that shares

some remarkable properties with the Lorenz system of equations

$$x_{n+1} = y_n + 1 - ax_n^2, \qquad y_{n+1} = bx_n . \tag{4.3.12}$$

Firstly this mapping has a *constant* Jacobian with the value $-b$, which according to Hénon is the natural counterpart of the constant divergence in the Lorenz equations (eq. (4.3.9)). For $|b| < 1$ the mapping is also area-contracting and some sort of attractor may be expected.

Secondly, the deformation with time of a volume in phase space in the Lorenz system that has been found in numerical solutions is carefully simulated by the Hénon equations. In his paper Hénon has shown further that the eqs. (4.3.12) are also the most *general* quadratic mapping with constant Jacobian.

By solving eqs. (4.3.12) numerically Hénon observed that the solutions tend towards a strange attractor and exhibit the usual corresponding behaviour. The structure of the attractor in the two-dimensional plane is such that a portion of it upon magnification shows a similar form as its surroundings: each apparent curve is made up of an infinity of quasi-parallel curves. See fig. 4.9.

This result gives an important clue to the question of the dimensionality of strange attractors. The absolute value of the Jacobian of the present example ($b = 0.3$) and its counterpart in the Lorenz equations show that a volume in phase space is continuously shrinking. Yet the solutions of both Hénon's and Lorenz' equations do not seem to tend towards a manifold of lower dimensionality than the phase space, as for example happens when point- or periodic attractors are present. Instead they seem to fill a finite portion of phase space but as fig. 4.9 shows probably not in a continuous manner. Loosely speaking the dimensionality of the Lorenz attractor is somewhere between 2 and 3, that of the Hénon attractor between 1 and 2.

Mathematical objects with similar properties are known as Cantor sets and an example may clarify the notion. Consider a straight line segment. Divide the line in three equal parts and 'take out' the middle part. Repeat this procedure at the remaining first and last part. And so on ad infinitum... The remaining structure is a Cantor set. It contains uncountably many points, is not continuous and is only 'dense' at certain points. The structure also repeats itself at each scale level. The analogy with the Hénon attractor is evident.

The difference between a strange attractor and the ordinary point and periodic attractors is the sensitivity to initial data in the former. This is indeed caused by generalised separatrices within the attracting part of phase space as was suggested above. Helleman gives a very lucid explanation of this [82]. He shows that in strange attractors there are infinitely long separatrices, intersecting each other in infinitely many points, while 'miraculously folding away their loops and plies within the strange bands of the attractor'. Hence every two points within the attractor are separated by the ubiquitous separatrices and thereby have completely different trajectories in phase space. Thus, for the non-linear gourmet a strange attractor is a spaghetti of separatrices.

Putting $b = 0$ in eqs. (4.3.12) and applying a simple linear transformation one finds back the first-order difference equation of section 4.2, known as the 'logistic' equation, which is still a further simplification, mapping a line segment onto itself. Yet, still the system has chaotic solutions for a certain parameter range.

At this point it is worthwhile considering how far we have actually gone from the original problem. Consider convection of a fluid between parallel plates, which by itself is a very rough physical model for the earth's atmosphere. The interaction of the particles in the fluid should be described by an ordinary differential equation for each particle, including all the physical interactions plus the influence of the physical boundaries. This system, which is untractable because of the large amount of particles involved,

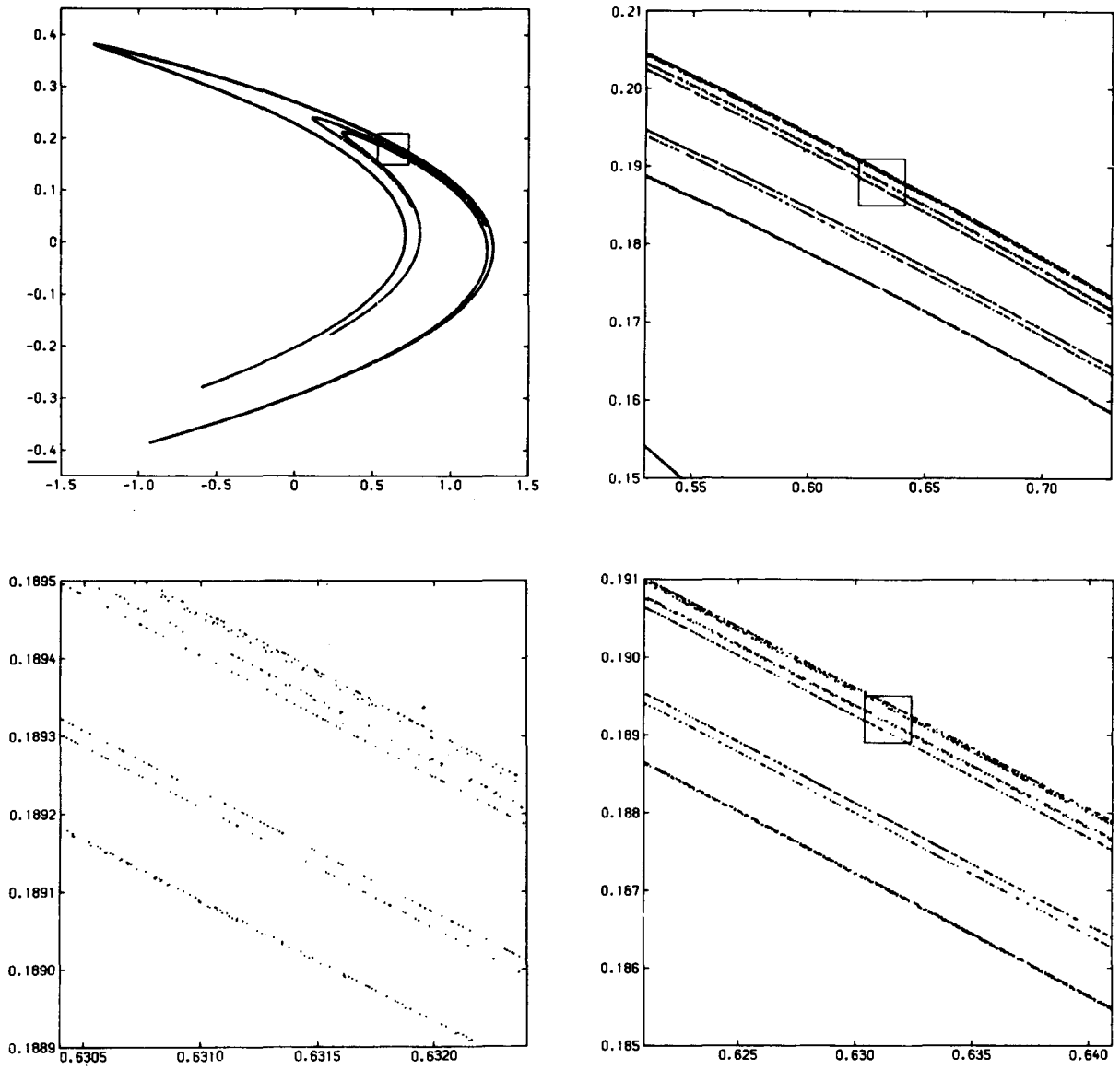

Fig. 4.9. The Hénon attractor. Each dot represents one interation of eq. (4.3.12) for the parameter values $b = 0.3$ and $a = 1.4$. Magnification of a portion of the attractor – clockwise from upper left – shows the same structure at increasingly deeper levels. From M. Hénon [88]. Courtesy of Communications in Mathematical Physics and the author.

is then replaced by a set of partial differential equations, treating the fluid as a continuum. From this system then only the interaction of the leading Fourier components in space is considered which results in truncated mode equations, in this case the Lorenz equations. The neglect of all but three Fourier terms is known to be incorrect in many cases (see above, ref. [80]) but important properties of the solutions may be preserved as was shown for a similar system of equations by Moore et al. [85], see the discussion above. Subsequently a Poincaré mapping is *defined* that mimics the truncated mode equations as well as possible and eventually this two-dimensional mapping is reduced to the one-

dimensional 'logistic' equation. Under all those transformations the qualities of sensitivity to initial data and aperiodicity are preserved. It is the intrinsic non-linearity that carries these properties along.

In conclusion of this section about strange attractors and chaotic behaviour I make a historical note. In experimental investigations of electrical circuits during the second world war Cartwright and Littlewood found chaotic behaviour. This was the motivation for them to study the solutions of the Van der Pol equation under periodic external forcing. (The Van der Pol equation describes electrical circuits.) In 1945, Cartwright and Littlewood published a paper [89] on the equation

$$\ddot{y} + k(1 - y^2)\dot{y} + y = b\lambda k \cos(\lambda t + a) \qquad (k \gg 1)\,. \tag{4.3.13}$$

This is a second-order non-autonomous differential equation, but it is trivially transformed into a third-order autonomous equation by introducing a new variable $z = \lambda t$ and adding the equation

$$\dot{z} = \lambda\,. \tag{4.3.14}$$

Chaotic behaviour is possible for this equation and is observed in numerical solutions (see Guckenheimer [90] for a more extensive description). However, the chaotic region is often not attracting and most orbits end up in stable limit cycles, which are *phase locked* with the driving term, i.e. the period of the oscillation is an integer multiple of the driving period. Most of the interest was directed to this last phenomenon and the importance of the possibility of chaos has elapsed the physical and mathematical community for more than 25 years! The results of Lorenz in 1963 [77] also remained largely unnoticed until the paper by Ruelle and Takens in 1971 [67]. At that time even these latter authors did not know of Lorenz' work.

4.4. Chaos in conservative systems

In conservative systems the possibility of chaotic solutions has been known for even a longer time. Poincaré [91] and Einstein [92] published papers on the subject in 1882 respectively 1917. They both pointed attention to the relation between chaotic solutions and the non-existence of analytically expressable integrals of motion, but apparently the physics community was not yet ready to appreciate the full consequences.

The difference between conservative systems and dissipative systems such as the ones in the previous sections is that in a conservative system the volume in phase space is rigorously conserved. This implies that there is at least one integral of motion. In the case of Hamiltonian systems this is the energy. Hamiltonian systems are very important in astronomy because they describe the motions of stars in clusters and galaxies, the motions of the planets and the sun in the solar system and in general n-body systems (without tidal friction). In Hamiltonian systems there is always an even number of degrees of freedom because the equations of motion are *second*-order differential equations in each variable. The simplest case of a particle moving in a one-dimensional potential is described by an equation of motion of the form

$$\ddot{x} = -\partial V(x)/\partial x \tag{4.4.1}$$

where $V(x)$ is the potential. The phase space of this problem is two-dimensional. The above equation can always be reduced to an integral, whence it is said to be solved analytically. The result is

$$t - t_0 = \int_{x(t_0)}^{x(t)} \frac{dx^1}{\sqrt{2E - 2V(x^1)}} \tag{4.4.2}$$

with E denoting the – conserved – energy of the motion. The trajectory of the particle in phase space is completely characterised by the velocity and the position of the particle at a given time (x and $\dot{x}$), which also yield the energy.

A slightly more complicated set of equations, which should be well known to most astronomers, is that of the motion of a point particle in a gravitational field in three dimensions, for example the motion of the earth in the sun's gravitation field. In dimensionless form and Cartesian coordinates it is described by

$$\ddot{x}_i = -x_i/(x_1^2 + x_2^2 + x_3^2)^{3/2} \qquad (i = 1, 2, 3). \tag{4.4.3}$$

This set of equations may be solved analytically and yields five integrals – energy, the three components of the angular momentum and the direction of the perihelion – which completely describe the motion in phase space, and in real space. The position of the planet is then found given the time of the last perihelion passage or the position at any other time. Although eqs. (4.4.3) form a sixth-order system there is not the least hint of chaos. The trajectories in phase space are all neatly closed curves, or run to infinity.

I will now use an example that is of even lower dimensionality than the one above to indicate the relation between chaos and the non-existence of analytically expressable integrals. The example was published in 1964 by Hénon and Heiles [87] and it has an astronomical background.

Hénon and Heiles considered the motion of a test star in a galaxy under the influence of the gravitational potential from the other stars of the galaxy. In cylindrical coördinates and with $U(r, \theta, z)$ denoting the gravitational potential, the equations of motion for the test star are

$$\begin{aligned} \ddot{z} &= -\partial U/\partial z \\ \ddot{r} &= -\partial U/\partial r + r\dot{\theta}^2 \\ \ddot{\theta} &= -\frac{1}{r^2}\frac{\partial U}{\partial \theta} - \frac{2\dot{r}\dot{\theta}}{r}. \end{aligned} \tag{4.4.4}$$

The gravitational potential is assumed symmetric around the z-axis ($\partial U/\partial\theta = 0$) and hence two integrals of motion can be found: the total energy and the z-component of the angular momentum

$$\begin{aligned} E &= U(r, z) + \tfrac{1}{2}(\dot{r}^2 + r^2\dot{\theta}^2 + \dot{z}^2) \\ L_z &= r^2\dot{\theta}. \end{aligned} \tag{4.4.5}$$

The second integral may be used to reduce the problem to a two-dimensional form. After the introduction of a new potential

$$V(r, z) = U(r, z) + L_z^2/2r^2 \tag{4.4.6}$$

the equations of motion reduce to

$$\ddot{r} = -\partial V/\partial r, \qquad \ddot{z} = -\partial V/\partial z . \tag{4.4.7}$$

Apparently the problem considered is completely equivalent to that of the motion of a particle in a plane with an arbitrary potential V. Hénon and Heiles *chose* the following potential for a detailed study. They assumed that it was a typical example of the general case (x and y replace r and z)

$$V(x, y) = \tfrac{1}{2}(x^2 + y^2) + x^2 y - y^3/3 . \tag{4.4.8}$$

The remaining integral is the energy, in the present notation

$$E = \tfrac{1}{2}(\dot{x}^2 + \dot{y}^2) + V(x, y) . \tag{4.4.9}$$

This equation can be used to eliminate one of the remaining variables, for instance x, and thus the equations of motion are reduced to a third-order system with a tunable parameter E, by which means the 'standard' form of the previous section is recovered. The resulting equations are

$$\begin{aligned} \mathrm{d}y/\mathrm{d}t &= \dot{y} \\ \frac{\mathrm{d}\dot{y}}{\mathrm{d}t} &= -y + y^2 + \frac{\dot{x}^2 + \dot{y}^2 + y^2 + \frac{2}{3}y^3 - 2E}{2y + 1} \\ \mathrm{d}\dot{x}/\mathrm{d}t &= \mp\sqrt{(\dot{x}^2 + \dot{y}^2 + y^2 + \tfrac{2}{3}y^3 - 2E)\,(2y + 1)} . \end{aligned} \tag{4.4.10}$$

The sign in the expression $\mathrm{d}\dot{x}/\mathrm{d}t$ changes as the right hand side becomes zero, provided that the second derivative of $\dot{x}$ is not zero at the same time.

In contrast with the equations of the previous section this system of equations is not dissipative, i.e. a volume element in phase space does not shrink continuously. Hence there are no attractors in this problem, but this does not exclude the existence of separatrices and accordingly the possibility of sensitivity to initial data and non-periodic orbits (see Helleman for an extensive discussion [82]).

Figure 4.10 shows the results of the numerical calculations. Each dot in the figure represents the intersection of a trajectory with the plane y, $\dot{y}$. For the lowest energy, $E = 1/12$, several trajectories with different initial conditions have been used. Each trajectory tends to remain on a closed curve in the $y,\dot{y}$-plane, indicating that it is confined to a torus in phase space. This would mean that there is a third integral of motion that determines these tori. For a slightly higher energy, $E = 1/8$, some tori seem to remain, but chaotic regions become evident. The random dots between the island are generated by *one* orbit. At $E = \frac{1}{6}$ the dots represent the trajectory of *one* point. Apart from some very small persistent islands the motion is now truly chaotic. For $E > \frac{1}{6}$ the equipotential lines open and the test star can escape to infinity.

It is curious that for small values of the energy a third integral of motion seems to exist although a well-known theorem of Poincaré [91] in 1892 claims the non-existence of an analytical third integral of motion. Gustavson [93] derived an expression for the third integral as a power series in the variables, but the convergence of the series cannot be proven. For small values of E Gustavson's results predict correctly the numerically calculated tori in fig. 4.10, but the correspondence gradually worsens as the energy increases.

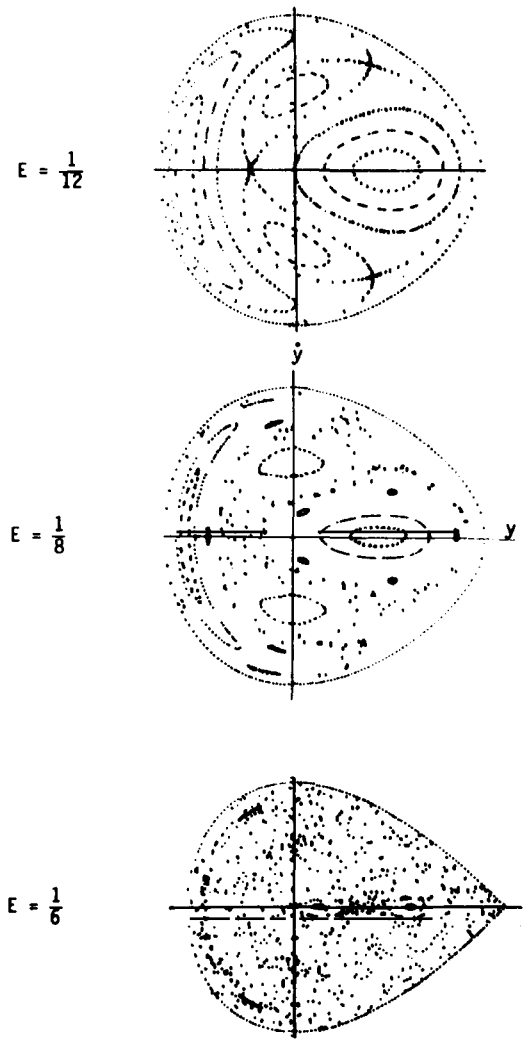

Fig. 4.10. The solutions of the Hénon–Heiles equations (4.4.10) in the $y,\dot{y}$-plane. Each dot represents the intersection of an orbit and the plane. The dots at $E = 1/6$ are generated by one orbit. This figure is from F. Gustavson [93]. Courtesy of the Astronomical Journal.

The sudden appearance of chaotic regions in phase space as E increases further cannot be explained at all with this power series. It is tempting, however, to identify this onset of stochasticity with the breakdown of the convergence of the power series.

In the Hénon–Heiles system, just as in dissipative systems, the transition from order to chaos takes place as the magnitude of the tunable parameter – the energy of the test star in this case – is increased. This has interesting consequences for the motions of stars in galaxies. The motion of low energy stars is likely to be confined to some periodic orbit, while high energy stars may wander around unpredictably in the galaxy. Since the stars in a galaxy probably have some smooth energy distribution order and chaos are expected to coexist.

4.5. Applications in astronomy

As far as conservative systems are concerned one can hardly speak of applications of methods of

non-linear dynamics since some of the pioneering work on chaotic behaviour comes from the study of stellar systems. The Hénon–Heiles equations have become the canonical example of the onset of stochasticity in statistical mechanics. Since non-linear stellar dynamics has become a full grown field of astronomy I cannot do it justice in just a few sentences and therefore I refer to a review on 'Integrable and stochastic behaviour in dynamical astronomy', by Contopoulos [94].

Strange attractors arise in dissipative systems under external forcing, for example with an external source of energy. The solar magnetic field is an example of such a system in which magnetic field is continuously dissipated or expelled into interplanetary space, while it is regenerated by the dynamo-action.

Zel'dovich and Ruzmaikin [95] have recently produced a simple extension of the usual kinematic dynamo equations to a form which also describes the non-linear suppression of the so-called α effect by the Lorentz forces in the convection zone. The resulting equations are *exactly* the Lorenz equations described in section 4.3 and for the parameter values appropriate for the solar case the model successfully reproduces the 'noisy' 11-year cycle in sunspot number, the field reversal at the end of each cycle and the periods of reduced solar magnetic activity, such as the Maunder, Spörer and Mediaeval minima (Eddy [96 and 97]).

The apparent 'noisyness' of the solar cycle – i.e. the small variations in amplitude and period of the sunspot number cycle – as well as the periods of reduced activity are not well explained by the standard strictly periodic solutions, which result from the *linear* dynamo equations, but they arise naturally when the solar cycle is described in terms of a strange attractor, or, more specifically, a Lorenz attractor.

In the following I will briefly sketch the derivation of the model equations of Zel'dovich and Ruzmaikin. For a thorough description of the dynamo theory I refer to recent reviews by Weiss [98] and Priest [99].

The full dynamo problem consists of solving the induction equation

$$\partial \boldsymbol{B}/\partial t = \nabla \times (\boldsymbol{v} \times \boldsymbol{B}) + \eta \Delta \boldsymbol{B} \tag{4.5.1}$$

and the momentum equation

$$\rho \, \mathrm{d}\boldsymbol{v}/\mathrm{d}t = -\nabla p - \rho \boldsymbol{g} + \boldsymbol{j} \times \boldsymbol{B} \tag{4.5.2}$$

together with an appropriate energy equation and the continuity equation. Here $\boldsymbol{B}$ is the magnetic field, $\boldsymbol{v}$ the plasma velocity, ρ the density and p the pressure, while $\boldsymbol{j}$ represents the current, $\boldsymbol{g}$ the gravitational acceleration and η the resistivity. Closure of the system is obtained by using the gas law and the remaining MHD equations

$$\nabla \cdot \boldsymbol{B} = 0 \tag{4.5.3}$$

$$\boldsymbol{j} = \frac{1}{4\pi} \nabla \times \boldsymbol{B}. \tag{4.5.4}$$

Usually only the *kinematic* dynamo problem is considered, which consists of solving the induction equation (4.5.1) for a given velocity field.

In the models for the solar dynamo frequently axisymmetry is assumed ($\partial \phi = 0$) together with constant density, which reduces the continuity equation to

$$\nabla \cdot \boldsymbol{v} = 0. \tag{4.5.5}$$

It is convenient to split the velocity field in poloidal and toroidal components

$$\boldsymbol{v} = (v_\phi \hat{\boldsymbol{\phi}}, \boldsymbol{v}_\mathrm{p}) . \tag{4.5.6}$$

An appropriate gauge for axisymmetric $\boldsymbol{B}$ is

$$\boldsymbol{B} = B\phi\hat{\boldsymbol{\phi}} + \nabla \times (A\hat{\boldsymbol{\phi}}) . \tag{4.5.7}$$

The vanishing divergence of the velocity field is used to write the toroidal component of the equation as

$$\partial B_\phi/\partial t + r\boldsymbol{v}_\mathrm{p} \cdot \nabla(B_\phi/r) = r\boldsymbol{B}_\mathrm{p} \cdot \nabla(v_\phi/r) + \eta(\Delta - 1/r^2)B_\phi \tag{4.5.8}$$

The first term on the right hand side shows how a shear in angular velocity results in the conversion of toroidal field into poloidal field, the so-called ω-effect ($\omega = v_\phi/r$). For the poloidal component one finds

$$\partial \boldsymbol{B}_\mathrm{p}/\partial t = \{\nabla \times (\boldsymbol{v} \times \boldsymbol{B})\}_\mathrm{p} + \eta\{\Delta \boldsymbol{B}\}_\mathrm{p} \tag{4.5.9}$$

where $\{\ldots\}_\mathrm{p}$ means the poloidal component of the vector between brackets. With (4.5.3) and (4.5.7) this yields

$$\nabla \times \left(\frac{\partial A}{\partial t}\hat{\boldsymbol{\phi}}\right) = \{\nabla \times (\boldsymbol{v} \times \boldsymbol{B})\}_\mathrm{p} - \eta\{(\nabla \times (\nabla \times \boldsymbol{B})\}_\mathrm{p} \tag{4.5.10}$$

which, because of axisymmetry, reduces to

$$\partial A/\partial t = (\boldsymbol{v} \times \boldsymbol{B}) \cdot \hat{\boldsymbol{\phi}} - \eta[\nabla \times \{\nabla \times (A\hat{\boldsymbol{\phi}})\}] \cdot \hat{\boldsymbol{\phi}} + c(t) . \tag{4.5.11}$$

$c(t)$ is an arbitrary function. Choosing $c(t) = 0$ and further working out this expression one finds

$$\frac{\partial A}{\partial t} + \frac{\boldsymbol{v}_\mathrm{p}}{r} \cdot \nabla(rA) = \eta\left(\Delta - \frac{1}{r^2}\right)A . \tag{4.5.12}$$

This equation shows no poloidal field is generated from toroidal field and consequently (4.5.12) implies that the whole magnetic field decays away, because of the diffusion terms on the right hand sides of (4.5.8) and (4.5.12). Therefore in a strictly axisymmetric medium no dynamo is possible, which is the essence of Cowling's theorem [100]. Note that the incompressibility has not been used in the derivation of eq. (4.5.12) so the theorem is quite universal.

For the solar dynamo problem this need not cause concern because the cellular convection in the solar interior results in a non-axisymmetric velocity field. Parker [101] was the first to propose a mechanism for the conversion of toroidal to poloidal flux by considering a rising cell of plasma in the convection zone. As the cell rises it expands and starts to rotate because of the Coriolis force. This twisting motion converts poloidal field lines to toroidal ones. In sinking cells the sense of rotation due to the Coriolis force is reversed and the generated toroidal field is of opposite direction. Consequently the net effect of rising and sinking motions would average out if these motions were symmetric. There is however an important asymmetry because of the stratification: rising cells expand, while falling cells

contract. Hence there exists a mechanism for converting toroidal field lines to poloidal ones in the solar convection zone. The rate of generation of poloidal field is proportional to the toroidal field and therefore Parker modelled the effect by adding a term proportional to B_ϕ at the right hand side of eq. (4.5.12)

$$\frac{\partial A}{\partial t} + \frac{\boldsymbol{v}_\mathrm{p}}{r} \cdot \nabla(rA) = \alpha B_\phi + \eta\left(\Delta - \frac{1}{r^2}\right)A\,. \tag{4.5.13}$$

This extra term describes the so-called α-effect: it presents the *mean* electric field over many cells. Therefore the vector potential A and toroidal B_ϕ in eqs. (4.5.8) and (4.5.13) from now also represent *averages* over a suitable length scale of many convection cells. There exist alternative ways to generate the α effect, but the magnitude of the constant α always depends on the value of the helicity of the velocity field: $\boldsymbol{v}\cdot(\nabla \times \boldsymbol{v})$. There is also an α-effect for the conversion of poloidal field to toroidal field, but for the solar case this effect is presumably much smaller than the ω-effect and therefore it will be neglected here. For further reference on the derivation of the kinematic dynamo equations see the reviews mentioned above, [98] and [99].

The kinematic dynamo equations (4.5.8) and (4.5.13) are *linear* in the magnetic field and may possess wave-like solutions which can account for the oscillation in sunspot numbers (the 11-year cycle), for the field reversal every 11 year and for the drift towards the equator of the sunspot belts (Spörer's law).

A problem for these types of waves is that they are decaying when α is smaller then a critical value α_c, growing without bound when $\alpha > \alpha_\mathrm{c}$ and have constant, but undetermined, amplitude when $\alpha = \alpha_\mathrm{c}$ (see Parker [102]). Usually this is resolved by assuming an effective α which depends on the amplitude of the oscillation, for example like

$$\alpha = \alpha_0 - CB^2\,. \tag{4.5.14}$$

When the amplitude of the oscillation becomes too large α is reduced below its critical value so the amplitude decays again and vice-versa. Actually this is a first attempt to model the effects of the non-linear terms in the momentum equations (4.5.2): due to the feedback of the Lorentz force on the velocity field the convection is suppressed and so is the α effect. A more subtle approach is found by studying the momentum equation in detail. The fact that this equation contains the first-order derivative of the velocity field implies that it takes some time for the Lorentz force to slow down the convection. Therefore since α depends directly on the helicity of the velocity field, instead of using a relation like (4.5.14) one may consider a relation like

$$\partial\alpha/\partial t = f(\alpha, B, \ldots) \tag{4.5.15}$$

with f a function to be determined, which accounts for the time needed to slow down convection. The (non-linear) term which causes the slow-down of convection is the acceleration due to the Lorentz force, which may be roughly modelled as

$$a_\mathrm{l} \approx AB_\phi/4\pi\rho L^2 \tag{4.5.16}$$

where ρ is the density and L the depth of the convection zone. Introducing ξ as the departure of α from its linear value (with $F_L = 0$) Zel'dovich and Ruzmaikin assume that α satisfies an equation of a very

simple type

$$\partial\xi/\partial t = -\xi/\tau_\alpha + AB_\phi/4\pi\rho L^2 \tag{4.5.17}$$

with τ_α the adjustment time scale, which accounts both for the reduction in α due to the Lorentz force in the convection zone and for the finite time needed for adjustment. This last equation is still an ad-hoc equation, but eq. (4.5.15) has really been derived by considering quasi-isotropic turbulence together with "kinetic" (field independent) helicity (Pouquet et al. [103] and Kliorin and Ruzmaikin [104]). Eq. (4.5.17) may then be considered as a first-order expansion of the full equation (4.5.15).

The next step in the analysis of Zel'dovich and Ruzmaikin is the assumption that the poloidal velocity field $\boldsymbol{v}_\mathrm{p}$ is so small that the terms containing it can be neglected in the induction equations. The influence of the terms containing the spatial inhomogeneities of the field is roughly modeled by introducing three time scales: τ_ϕ the diffusion time for the toroidal field, τ_p the same time scale for the poloidal field, and $\tau_\omega = 1/\omega$ the time scale for the ω-effect where ω is the rotation frequency of the sun. Hence

$$r\boldsymbol{B}_\mathrm{p}\cdot\nabla(v_\phi/r) \Rightarrow A\omega/L \tag{4.5.18}$$

$$\eta(\Delta - 1/r^2)B_\phi \Rightarrow -B_\phi/\tau_\phi \tag{4.5.19}$$

$$\eta(\Delta - 1/r^2)A \Rightarrow -A/\tau_\mathrm{p}\,. \tag{4.5.20}$$

In the first substitution the further approximation $|\boldsymbol{B}_\mathrm{p}| = |\nabla \times A\hat{\boldsymbol{\phi}}| \approx A/L$, has been made, where L is again the depth of the convection zone.

Thus we are left with three coupled first-order ordinary differential equations

$$\begin{aligned}
\partial B_\phi/\partial t &= A\omega/L - B_\phi/\tau_\phi \\
\partial A/\partial t &= \alpha_0 B_\phi - \xi B_\phi - A/\tau_\mathrm{p} \\
\partial\xi/\partial t &= -\xi/\tau_\alpha + AB_\phi/4\pi\rho L^2\,.
\end{aligned} \tag{4.5.21}$$

This systems of equations may *exactly* be reduced to the Lorenz system (4.3.7) by the following substitutions

$$\begin{aligned}
X &= B_\phi \times (\sqrt{4\pi\rho}\, L/\tau_\mathrm{p})^{-1} \\
Y &= A \times (\sqrt{4\pi\rho}\, L^2/\omega\tau_\phi\tau_\mathrm{p})^{-1} \\
Z &= \xi \times (L/\omega\tau_\phi\tau_\mathrm{p})^{-1} \\
\bar{t} &= t/\tau_\mathrm{p}\,, \qquad \sigma = \tau_\mathrm{p}/\tau_\phi\,, \qquad \alpha = \tau_\mathrm{p}/\tau_\alpha\,, \\
b &= \alpha_0\omega\tau_\mathrm{p}\tau_\phi/L\,.
\end{aligned} \tag{4.5.22}$$

We note that the remaining parameters σ and α represent ratios of diffusion times while the forcing parameter b is just the non-dimensional dynamo number known from linear theory (see Parker [102]).

The solutions of the Lorenz equations were discussed in section 4.3. With regard to the dynamo problem the most interesting solutions are those for which there exists a strange attractor. As was

shown in section 4.3 for $b > 1$ there are three static solutions: the origin and the points $(x, y, z) = (\pm\sqrt{\alpha(b-1)}, \pm\sqrt{\alpha(b-1)}, (b-1))$ which all turn unstable as b surpasses a certain threshold value. The solutions in the strange attractor regime exhibit a few rotations around one of the static points away from the origin and then quickly shift to the other 'wing' of the 'butterfly' attractor – see fig. 4.4 – where they rotate a few times around the other static point before quickly turning to the original 'wing' again. Every once in a while the solution lingers for some time around the origin (no such event is displayed in fig. 4.4). It was shown by Rabinovich [76] that for certain values of the parameters α, σ and b the transitions from one 'wing' to the other are quasi-periodic while the stay around the origin takes place at irregular intervals and has a length of several periods. Zel'dovich and Ruzmaikin identify the quasi-periodic transitions from one wing to the other with the field reversals in the sun once about every 11 years, the rapid oscillations around the static points with the variations in sunspot number and the irregular lingering of the solution around the origin with the gaps in the solar cycle, like the well-known Maunder, Spörer and Mediaeval minima.

These results show how the non-linear terms in the momentum equation may in principle account for the irregularities in the solar cycle. In the terminology set forth in the introduction this model is "ad hoc", since it contains no *strict* derivation. Its principal weakness is that the exact values of the time scales τ_ϕ, τ_p and τ_α are not very well determined, only their orders of magnitude are. Therefore it is interesting, but maybe not meaningful, to play with these parameters in order to reproduce observables like the 22-year periodicity or the duration of the Maunder minimum. The next step in the theory would be to determine the relevant time scales more accurately either from theory, numerical calculations or observable quantities in order to check whether the model gives the correct result for the parameter values thus derived.

Cattaneo et al. [105] have obtained similar results with a simple parameterised mean field dynamo model which includes the effect of the reduction of the differential rotation by the Lorentz force. Therefore, while Zel'dovich and Ruzmaikin model the suppression of the α-effect, these authors model the suppression of the ω-effect. The model consists of seven coupled non-linear ordinary differential equations. As the dynamo number increases the solutions of the equations change from static to strictly periodic and finally to chaotic. The chaotic solutions show again a basic imperfect cyclicity with periods of reduced activity. Cattaneo et al. conclude that Maunder minima are a characteristic feature of a wide class of non-linear dynamos.

It is interesting to note that in these non-linear dynamos, despite the strong cyclicity, all phase information of the cycle is gradually lost, in particular in the periods of reduced activity this process is rather quick. Therefore it is impossible to predict *exactly* the long term behaviour of the dynamo, only features as the basic periodicity and the duration of irregularities may be predicted.

A surprising and fascinating application of the results of non-linear dynamics is in the study of ideal MHD equilibria. Tsinganos, Distler and Rosner [106] have recently explored the formal analogy between the topology of the magnetic lines of force in coordinate space and the topology of integral surfaces of one- and two-dimensional Hamiltonians in phase space. They found that the Kolmogorov, Arnold and Moser (KAM) theorem, predicting stochastic particle trajectories in certain parts of phase space, applies here. The KAM theorem has not been discussed in this review, but see for example Helleman [82] for an extensive discussion or Arnold's book [107].

In magnetic field dominated astrophysical plasmas, such as the solar corona, the force balance for magnetostatic equilibrium is given by

$$\nabla p = \frac{1}{4\pi} (\nabla \times \boldsymbol{B}) \times \boldsymbol{B} \tag{4.5.23}$$

$$\nabla \cdot \boldsymbol{B} = 0 . \tag{4.5.24}$$

In many astrophysical applications the gradient of the gas pressure (∇p) is negligible compared with the Lorentz force and the governing equations reduce to that of force-free fields that were discussed in section 2.2 in the context of solar flares. Here the more general case described by the equations above will be considered.

Tsinganos et al. note that all available exact non-singular solutions of the system (4.5.23) and (4.5.24) have at least one ignorable coordinate, that is, for each equilibrium state there exists a generalised orthogonal coordinate system (x_1, x_2, x_3) such that $\partial/\partial x_3$ is zero everywhere. (However, it has not been proven yet, that this spatial symmetry is a *necessary* condition for equilibrium.) Magnetostatic equilibria with this spatial symmetry are characterized by two-dimensional flux surfaces $A(x_1, x_2)$ in three-dimensional configuration space on which the plasma pressure and the twist of the field lines are constant. It was shown by Kruskal and Kulsrud [108] that the only physically realizable topology for these flux surfaces is that of nested tori, on which the electric current and the plasma pressure are constants. The magnetic field can be expressed in terms of the flux function as

$$\boldsymbol{B} = \left(\frac{1}{h_2 h_3} \frac{\partial A}{\partial x_2}, \frac{-1}{h_1 h_3} \frac{\partial A}{\partial x_1}, \frac{f(A)}{h_3} \right) \tag{4.5.25}$$

with h_i the line element along the unit vector $\hat{\boldsymbol{x}}_i$ and $f(A)$ the field line 'twist'. Note that this field satisfies the continuity equation (4.5.24) identically.

Tsinganos et al. now construct a one-dimensional Hamiltonian

$$H(q, p) = A(x_1, x_2) \tag{4.5.26}$$

with time parameter

$$t = \frac{1}{f(A)} \int_{A=\text{constant}} \frac{h_3}{h_2 h_1} \mathrm{d}x_3 \tag{4.5.27}$$

which has the properties that the Lagrangian equation of motion for this Hamiltonian is the momentum equation (4.5.23) and that the Hamiltonian equations are the generating equations for the field lines. Evidently a flux surface coincides with an energy surface for the Hamiltonian (4.5.26) and further a field line is strictly equivalent to a particle trajectory for the Hamiltonian in p,q,t-space.

The existence of flux surfaces is essential in the derivation of this one-dimensional Hamiltonian. If for some perturbation there exist no new neighbouring flux surfaces at all, the equivalence with a one-dimensional Hamiltonian system ceases to exist. Therefore Tsinganos et al. use a procedure prescribed by Goldstein [109] to introduce a two-dimensional Hamiltonian which may describe the magnetostatic equilibrium after such perturbations.

The idea is to treat the time in the one-dimensional Hamiltonian (4.5.26) as an additional coordinate: $q_2 = t$. For that purpose the trajectories in phase space are marked with a parameter θ – for instance giving the arclength along the trajectory – which serves as the new independent variable. It can be proven (see Goldstein [109] p. 358) that the momentum conjugate to q_2 is then given by

$$p_2 = -H(q_1, p_1) \tag{4.5.28}$$

and the new Hamiltonian $H^{(2)}$ is:

$$H^{(2)}(q_1, q_2, p_1, p_2) = \frac{\mathrm{d}q_2}{\mathrm{d}\theta}\{H^{(1)}(q_1, p_1) + p_2\}\,. \tag{4.5.29}$$

This Hamiltonian contains the derivative of the function $t(\theta)$, namely $\mathrm{d}q_2/\mathrm{d}\theta$ – which has to be specified in advance – and is by construction independent of q_2 and θ. This two-dimensional Hamiltonian has to be considered in a formal way: the Hamiltonian equations of this system may be identified with the generating equations of the field lines, but it must be ignored that the Hamiltonian $H^{(2)}$ is by construction identically zero.

The – formal – Hamiltonian (4.5.29) is independent of θ and q_2 and is therefore conservative and has one cyclic coordinate. Consequently the solutions of this system lie on two-dimensional integral surfaces in the four-dimensional phase space. The integral surfaces of $H^{(2)}$ correspond to the flux surfaces $A(x_1, x_2)$ is constant.

This leads to the important conclusion that every non-singular stationary magnetostatic equilibrium with at least *one* ignorable coordinate corresponds to an *integrable* two-dimensional Hamiltonian system. In particular every field line corresponds to a particle trajectory. The incompressibility of the stream lines in phase space corresponds directly to the continuity of the field lines ($\nabla \cdot \boldsymbol{B} = 0$).

Using the formal equivalence described above Tsinganos et al. consider the question what happens when the symmetric magnetostatic equilibria are subject to perturbations lacking *any* symmetry. The equivalent problem for dynamical systems is studied by considering a perturbed Hamiltonian system

$$H^{(2)} = H_0^{(2)} + \varepsilon H_1^{(2)}\,, \tag{4.5.30}$$

where $H_0^{(2)}$ is the original integrable Hamiltonian describing the symmetric magnetostatic equilibrium, $H_1^{(2)}$ is an arbitrary non-integrable Hamiltonian and ε is a small but not necessarily infinitesimal number.

The celebrated KAM theorem ([82] and [107]) states that a *finite* measure of the integral surfaces of the original Hamiltonian is destroyed by the perturbation. This means that for certain values of the original flux parameter $A(x_1, x_2)$ the field lines no longer remain on the two-dimensional surface determined by $A(x_1, x_2)$. As the flux surfaces no longer exist in certain regions the isobaric surfaces for the plasma pressure also cease to exist, since the two coincide by the assumption of magnetostatic equilibrium. However, since the pressure gradient is by definition a conservative force it *must* possess isolaric surfaces and this conflicting demand leads to the conclusion that there cannot be any longer force balance everywhere and therefore that magnetostatic equilibrium ceases to exist.

This results in continuous motions in plasmas that are asymmetrically perturbed and enhanced dissipation as the magnetic field tries to regain its symmetrical equilibrium. Thus Parker's result [110] that magnetostatic equilibria are unstable against arbitrary infinitesimal perturbations is confirmed and extended to the domain of finite perturbations. Also it is shown that the intimate connection between magnetic fields and 'activity' in astrophysical plasmas may be quite fundamental as was already conjectured by Parker [102].

A final example of the use of non-linear dynamics in astronomy is that of stochastic ion acceleration by plasma waves, which is a plausible mechanism for second stage ion acceleration in solar flares, see Varvoglis and Papadopoulos [111]. Varvoglis has recently described the theoretical basis of this phenomenon [112]. He considers a test ion moving in the field of a linearly polarized magnetosonic wave of the form

$$B_1 = \frac{-k_\parallel}{k} B_1 \cos(k_\perp x + k_\parallel z - \omega t)\hat{x} + \frac{k_\perp}{k} B_1 \cos(k_\perp x + k_\parallel z - \omega t)\hat{z} \tag{4.5.31}$$

with $k_\parallel$ and $k_\perp$ denoting respectively the component of the wave vector k parallel and perpendicular to the background magnetic field $B_0\hat{z}$. The equations of motion of the test ions under the combined influence of the plasma wave and the background field can be written in the Hamilton form, with the Hamiltonian

$$H = \frac{1}{2m}\left(\boldsymbol{P} - \frac{q}{c}\boldsymbol{A}\right)^2 \tag{4.5.32}$$

where $\boldsymbol{A}$ denotes the vector potential of the total magnetic field $\boldsymbol{B}_0 + \boldsymbol{B}_1$ and q and m the charge and the mass of the test ion. Choosing an appropriate gauge the vector potential may be written as

$$\boldsymbol{A} = A_y\hat{y} = \hat{y}\left\{xB_0 + \frac{B_1}{k}\sin(k_\perp x + k_\parallel z - \omega t)\right\}. \tag{4.5.33}$$

This leads directly to a form of the Hamiltonian to which 'standard' non-linear theory is applicable

$$H = H_0 + \varepsilon H_1 + \varepsilon^2 H_2 \tag{4.5.34}$$

with ε being a measure for the amplitude of the plasma wave

$$\varepsilon = \frac{k_\perp}{k}\frac{B_1}{B_0}. \tag{4.5.35}$$

It is easily verified that in the zero-order Hamiltonian y and z are cyclic coordinates and therefore that P_y and P_z are conserved quantities. Consequently the solutions of the equation when projected onto the x,P_x-plane perform rotations on circles, the radius of the circle being the conserved energy of the motion (see fig. 4.11).

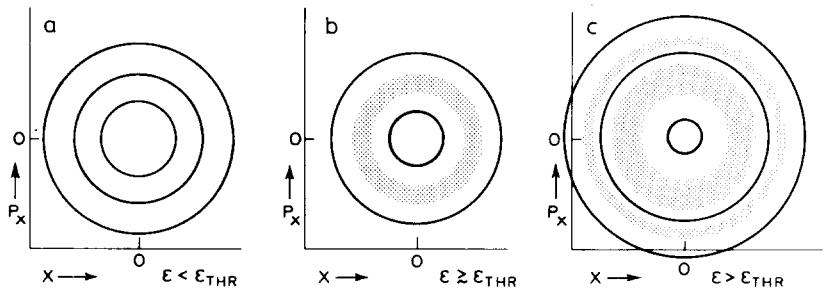

Fig. 4.11. Schematic drawing of the solutions of the Hamiltonian system eq. (4.5.34), as a function of the dimensionless wave amplitude ε. a) represents the projection of the solutions for $\varepsilon < \varepsilon_{thr}$ in the x,P_x-plane: the results are circles around the origin. b) represents solutions for ε just above the threshold value. The dots in the chaotic annulus represent the intersection of one trajectory with the x,P_x-plane. The drawn curves also represent the intersections of one trajectory with the plane: the dots are so close together that a regular curve appears. c) the solutions for ε well above the threshold value: the original chaotic annulus has grown and a new chaotic annulus has appeared.

For $\varepsilon > 0$, y remains a cyclic coordinate and P_y remains conserved. The motion of the test ion is therefore restricted to a four-dimensional phase space (x, z, P_x, P_z). A transformation to the wave frame $(z' = z - (\omega/k_\parallel)t$ and $P'_z = P_z - m\omega/k_\parallel)$ eliminates the explicit time dependence of the Hamiltonian. Therefore the energy of the test ion in the wave frame is constant. This restricts its motion to a three-dimensional subspace of the four-dimensional configuration space, labelled by the value of the energy of the particle. I stress here that the conservation of energy in the wave frame does *not* imply conservation of energy in the plasma frame; on the contrary, the rapid loss of energy of the wave to the ions is the most salient result of this analysis.

As was mentioned above there exists a second integral of motion for the zero-order Hamiltonian, which restricts the motion to two-dimensional tori in the four-dimensional configuration space. The cross sections of these tori with the x,P_x-plane are the solution curves of fig. 4.11a. When ε increases from zero the solutions first remain restricted to two-dimensional tori, which are slightly deformed versions of the original ones, but as ε surpasses a certain threshold one of the tori is destroyed and the corresponding orbits wander stochastically in its neighbourhood. In the x,P_x-plane a chaotic annulus has originated, with each dot indicating an intersection of a particle trajectory with the plane (see fig. 4.11b). Outside this annulus the orbits remain regular. As ε increases further the chaotic annulus spreads – mainly outwards – and new chaotic annuli emerge outside the first one. A further increase in ε causes the annuli to spread and finally merge with the original one, while more annuli are created outside it. Thus the chaotic part of phase space grows larger and larger.

This behaviour is clearly analogous to the origin of chaotic behaviour in the similar Hénon–Heiles system (section 4.4). It is different, however, in the detailed evolution of the chaotic parts of phase space as ε increases. This is typical for non-linear Hamiltonian systems of these types: there are strong overall patterns with regard to the origin of chaos, but the details of the evolution differ considerably.

The astronomical application of the chaotic test ion trajectories as a result of particle wave interaction is that it is a very efficient mechanism for accelerating ions and consequently also for damping waves. Consider a test ion with low energy originally gyrating undisturbed in the magnetic field. Suppose now that a plasma wave passes of sufficiently high amplitude and that the particle's original orbit is within the chaotic annulus, near the inner boundary. The numerical results of Varvoglis [112] show that such a particle may wander stochastically to the outer radius of the annulus in only a few gyration times. For $\varepsilon = 0.4$ Varvoglis thus found a thousandfold increase in the energy of the ion in those few gyration times! This is truly a strong acceleration. If the energy distribution of a sample of ions is such that most of the ions have an energy comparable to that which corresponds to the inner boundary of the annulus, very strong heating and very strong damping of the plasma waves result. Detailed application of this mechanism to the solar coronal setting is now under consideration see for example [111].

In conclusion of this section I will speculate about the possibilities for chaotic behaviour in stellar winds. There is a small hint on this possibility in the work of Hearn, Kuin and Martens [47], discussed in section 3.4.

It might be that the relaxation oscillation found in this paper is the first of a sequence of period doubling bifurcations: a Feigenbaum sequence (see section 4.2). Large scale stochastic behaviour is then expected at the point of convergence of the period doubling sequence. Therefore it will be interesting to increase the value of the forcing parameter – the acoustic flux in this case – and see whether and where a second bifurcation occurs. Using the universality of the Feigenbaum sequence one may then predict the value of the forcing parameter at which large scale chaos sets in. This is important because without this general idea numerical solutions exhibiting chaotic behaviour would probably be attributed to deficien-

cies in the computer program and be disregarded. The observations discussed in the paper of Hearn et al. do suggest chaotic behaviour and the gasdynamic equations that describe stellar coronae and winds are indeed very similar to the usual hydrodynamic equations for which chaotic solutions are known to exist. The major difference between the two sets of equations is that the stellar wind equations explicitly allow for a density stratification, but this is an additional complexity, which presumably only makes the solutions more complex in behaviour and does not destroy the possibilities already existent.

5. Conclusions

Catastrophes, bifurcations and strange attractors are all intrinsically related with non-linearities. Linear differential equations may be solved analytically and therefore the motion of particles in phase space is on well defined curves. That this is not always the case in non-linear systems is a discovery of great importance that has major implications for our view on physics. It goes against most people's intuition to think that there are processes that are *completely deterministic* and yet *intrinsically unpredictable* in the long run. The inability to make long run accurate predictions for every day matters such as the weather or the economy is usually ascribed to inadequate computer facilities (in meteorology) or inadequate theoretical foundations for such computations (in economy). Yet, simple mathematical models, such as the ones in this paper, show that unpredictability may have more profound reasons. The key is sensitivity to initial data, a phenomenon that can beat any computer. I will give a final very simple example of this, due to Lauwerier [113], to convince even the most reluctant computer fanatic. Consider the following procedure, which anyone can program on a computer:

1. Start with an arbitrary number between zero and one.
2. Multiply this number by two and subtract one if the result is larger than unity. (The result is again smaller than unity.)
3. Repeat this procedure on the outcome.
4. And son on...

In the computer's 'mind' a number looks like a sequence of zeros and ones: 0.110....010, whatever the number of digits is that the computer can handle. Multiplication by two in this notation just means that every digit shifts one position to the left, so the result is 1.10....010? It depends on the specific computer that is used whether the last digit is a zero or a one and probably this number is arbitrary. After only a few iterations, exactly as many as the number of digits that the computer can handle, the result of the iteration has become totally unpredictable from the initial value. Yet from one iteration to the next the result is very accurate. No matter how good the computer is, it cannot predict the result on the long run.

The apparent paradox of deterministic equations with unpredictable outcomes may be best explained in general with the concept *determinability* introduced by Born in 1955 [114] (see also Rabinovich [76] for a discussion). In physical experiments, due to the always limited precision of measurements and in numerical simulations, due to the finite precision of any computer, an initial state of a certain system is always determined within a possibly very small, but always finite, uncertainty ε.

Now the deterministic nature of the evolution equations of a given system tells us that for any given initial value $X(t_0) - X$ may represent a number, a vector, a function, or sets of these – there is a unique solution, or trajectory in phase space. In order words: there is a one-to-one transformation $X(t_0) \rightarrow X(t)$ for any $t > t_0$, also for $t \rightarrow \infty$. In view of the finite uncertainty in any experiment or computation the deterministic nature of the evolution equations means that after taking the limit $\varepsilon \downarrow 0$ – and thus

determining the initial state exactly – one may predict the state of the system at any time and therefore take the limit $t \to \infty$.

The prevalent intuitive notion on deterministic systems is that these limits may be reversed, i.e. first take the limit $t \to \infty$ then $\varepsilon \downarrow 0$ and thus find the final state of the system. This is also the only possibility in actual experiments because taking the limit $\varepsilon \downarrow 0$ is impossible and therefore must be postponed to the end of the measurement or the calculation. Implicitly it is then assumed that trajectories that start within some ε-neighbourhood of the 'real' initial value will stay close to the trajectory of the 'real' solution. Sensitivity to initial data means that this assumption is *not* correct: the trajectories emanating from any ε-neighbourhood, however small, always diverge and end up at finite distances. In the dissipative case they outline a strange attractor after some time (see fig. 4.5). In the non-dissipative case they may fill the whole phase space.

In Born's terminology the outcomes of the evolution equation are *determinable* when the limiting procedures $\varepsilon \downarrow 0$ followed by $t \to \infty$ may be reversed, and *undeterminable* when the limits may not be reversed.

In my view the intuitive difficulty that many people have in accepting deterministic evolution equations and unpredictable outcomes stems from the heavy emphasis – not to say indoctrination – put on exactly solvable problems in almost all (under) graduate courses in mathematics and physics. This emphasis, although understandable and almost unavoidable in the pre-computer era, need not persist in this time. Anyone can solve the 'logistic' equation (section 3.2) on a pocket-calculator and any undergraduate student can solve the Lorenz system (section 3.3) as an exercise in computer programming. I think it will change their intuitive notions.

The idea of non-determinability of outcomes of deterministic evolution equations may even have interesting consequences for matters outside the physical sciences. Capitalist and Marxist ideologies tell us that the laws of the free-market economy and the laws of history lead *inevitably* to an optimally functioning economy and society or to the installation of socialism as the ultimate political/economical system respectively. Apart from the issue of the validity of these laws the possibility could be considered that the knowledge of the laws that govern the evolution of the society may not lead to substantial predictive power on the evolution of society! Just as the knowledge of the equations of hydrodynamics does not permit meteorologists to predict weather for more than a week in advance, no matter how precise their data are on the initial state of the atmosphere. For systems like the earth's atmosphere, scientific research cannot go further than forecasting averages (e.g. July is warmer than January) or specific patterns (e.g. the alternation of cyclones and anti-cyclones), but the detailed long term evolution of these systems is unforseeable.

The application of the methods of non-linear dynamics in astronomy is still in a pioneering phase, except from the field of stellar dynamics which even led the way in the genesis of non-linear dynamics. However, I do not doubt that astronomy is a potentially very rich source of problems that are tractable with the theory outlined in this review. The use of non-linear methods and their results in other disciplines may therefore be a stimulus for astronomical research. This review has been an attempt to contribute to this purpose.

Acknowledgements

This paper has grown out of my thesis research on the applications of non-linear differential equations in astrophysics. Prof. Dr. H.G. van Bueren and Dr. J.M.E. Kuijpers, two of my thesis

advisers, in 1979 felt the time had come to use the results and techniques of non-linear dynamics and fluid dynamics in astrophysics and right they were, considering the large amount of papers that has appeared since in this particular field.

The first draft of this paper, describing the methods of non-linear dynamics, served as an introduction to my thesis, which I completed in January 1983. In the present version of the paper much material has been added concerning the astrophysical applications of these methods, including my own thesis research on non-linearity in stellar coronae. Most of the latter research was performed under the guidance of and in cooperation with Prof. A.G. Hearn, my third thesis adviser.

This paper has improved much because of the critical reading and useful comments of my thesis advisers and of Dr. P. Hoyng who took interest in this work in a later stage and carefully read the final version.

It is a pleasure to express my gratitude of the persons mentioned above, to Evert Landré and Hans Braun who prepared all the figures and to Louise Cramer and Irma Merkestein who did most of the typing.

Part of this work was supported by the Netherlands Foundation for Astronomical Research (ASTRON) with financial aid from the Netherlands Organization for the Advancement of Pure Science (ZWO).

References

[1] E.C. Zeeman, Catastrophe Theory, Selected Papers 1972–1977 (Addison-Wesley, 1977).
[2] E.C. Zeeman, Catastrophe theory, Scient. Am. 234 (4) (1976) 65–83.
[3] T. Poston and I. Stewart, Catastrophe Theory and its Applications (Pitman, London, 1978).
[4] R. Thom, Stabilité Structurelle et Morphogenèse, Mathematical Physics Monograph Series (Benjamin, Reading, 1972).
[5] W. van Tend and M. Kuperus, The development of coronal electric current systems in active regions and their relation to filaments and flares, Sol. Phys. 59 (1978) 115–127.
[6] W. van Tend, A model for solar flare energy build-up, in: Pleins Feux sur la Physique Solaire, Colloque International No. 282 du C.N.R.S. (Editions du C.N.R.S., 1978) pp. 227–231.
[7] B.C. Low, Nonlinear force-free magnetic fields, Rev. Geophys. and Space Phys. 20 (1982) 145–159.
[8] R. Rosner, W.H. Tucker and G.S. Vaiana, Dynamics of the quiescent solar corona, Astrophys. J. 220 (1978) 643–665.
[9] A.W. Hood and E.R. Priest, The equilibrium of solar coronal magnetic loops, Astron. Astrophys. 77 (1979) 233–251.
[10] A.W. Hood and E.R. Priest, Solar flares: Magnetohydrodynamic instabilities, in: Solar Phenomena in Stars and Stellar Systems, NATO Advanced Study Institute (1980, Bonas, France), eds. R. Bonnet and A.K. Dupree (Reidel, Dordrecht, 1981) pp. 509–532.
[11] P.C.H. Martens and N.P.M. Kuin, On cool coronal loops, Astron. Astrophys. 112 (1982) 366–368.
[12] R.W.P. McWirther, P.C. Thoneman and R. Wilson, The heating of the solar corona II. A model based on energy balance, Astron. Astrophys. 40 (1975) 63–73.
[13] J.C. Raymond, D.P. Cox and B.W. Smith, Radiative cooling of a low-density plasma, Astrophys. J. 204 (1976) 290–292.
[14] J.A. Ionson, Resonant electrodynamic heating of stellar coronal loops: an LRC-circuit analog, Astrophys. J. 254 (1982) 318–334.
[15] P.C.H. Martens and M. Kuperus, Resonant electrodynamic heating and the thermal stability of coronal loops, Astron. Astrophys. 113 (1982) 324–327.
[16] P.C.H. Martens and M. Kuperus, A thermal catastrophe in a resonantly heated coronal loop, in: Solar and Stellar Magnetic Fields: Origins and Coronal Effects, IAU-Colloquium 102, ed. J.O. Stenflow (Reidel, Dordrecht, 1983) pp. 397–400.
[17] N.A. Krall and S.K. Antiochus, The evolution of active region loop plasma, Astrophys. J. 242 (1980) 374–382.
[18] I,J.D. Craig and A.N. McClymont, The dynamic formation of quasi-static active region loops, Sol. Phys. 70 (1981) 97–113.
[19] R. Howard and Z. Švestka, Development of a complex of activity in the solar corona, Sol. Phys. 54 (1977) 65–105.
[20] R.H. Levine and G.L. Withbroe, Physics of an active region loop system, Sol. Phys. 51 (1977) 83–101.
[21] P.C.H. Martens and N.P.M. Kuin, The thermal evolution of resonantly heated coronal loops, Astron. Astrophys. 123 (1983) 216–224.
[22] P. Hut, Stability of tidal equilibrium, Astron. Astrophys. 92 (1980) 167–170.
[23] V.A. Antonov, Vest. Leningr. Univ. 7 (1962) 135–147 (article in Russian, summary in English).
[24] D. Lynden-Bell and R. Wood, The gravo-thermal catastrophe in isothermal spheres and the onset of red-giant structure for stellar systems, Mon. Not. R. Astr. Soc. 138 (1968) 495–525.

[25] J. Katz, On the number of unstable modes of an equilibrium, Mon. Not. R. Astr. Soc. 183 (1978) 765–769.
[26] J. Demaret, V. Dzuba and J. Perdang, The stellar dynamical catastrophe, Astron. Astrophys. 70 (1978) 287–296.
[27] G. Iooss and D.D. Joseph, Elementary Stability and Bifurcation Theory, Undergraduate Texts in Mathematics (Springer, Berlin, 1980).
[28] C. Jacobi, Uber die Figur des Gleichwichts, Poggend. Annal. 33 (1834) 229–232.
[29] H. Poincaré, Sur l'equilibre d'une masse fluide animeé d'un mouvement de rotation, Acta Math. 7 (1885) 259–380.
[30] I. Stakgold, Branching of solutions of non-linear equations, SIAM Rev. 13 (1971) 289–332.
[31] E. Hopf, Abzweigung einer Periodischen Lösung von einer Stationären Lösung eines Differentialsystems, Berichte über die Verhandlungen der Sächsischen Akademie der Wissenschaften zu Leipzig, Mathematisch-Physischen Klasse XCIV, 1 (1942) 3–22.
[32] F.H. Busse, Transition to turbulence in Rayleigh–Bénard convection, in: Hydrodynamic Instabilities and the Transition to Turbulence, Topics in Applied Physics 45, eds. H.L. Swinney and J.P. Gollub (Springer, Berlin, 1981) pp. 97–138.
[33] H.L. Swinney and J.P. Gollub (eds.), Hydrodynamic instabilities and the transition to turbulence, Topics in Applied Physics, Vol. 45 (Springer, Berlin, 1981).
[34] M.M. Vainberg and V.A. Trenogin, The methods of Lyapunov and Schmidt in the theory of nonlinear equations and their further development, Russ. Math. Surveys 17(2) (1962) 1–60.
[35] J. Carr, Applications of Centre Manifold Theory, Applied Mathematical Sciences 35 (Springer, Berlin, 1982).
[36] N.R. Lebovitz, Bifurcation and stability problems in astrophysics, in: Applications of Bifurcation Theory, ed. P.H. Rabinovitz (Acad. Press, New York, 1977) pp. 259–284.
[37] W. Thomson (Lord Kelvin) and P.G. Tait, Treatise on Natural Philosophy (Cambridge University Press, 1883).
[38] A. Lyapunov, Sur un Problème de Tchebychef, Mémoires de l'Academie de St. Petersbourg XVII 3 (1905).
[39] J.H. Jeans, Astronomy and Cosmogony (Cambridge University Press, 1929; Dover Publications, 1961).
[40] D. Lynden-Bell, On large-scale instabilities during gravitational collapse and the evolution of shrinking MacLaurin Spheroids, Astrophys. J. 139 (1964) 1195–1216.
[41] N.R. Lebovitz, On the fission theory of binary stars, Astrophys. J. 175 (1972) 171–183.
[42] R. Wiegandt, The equilibrium and bifurcation of rotating stellar systems, Astron. Astrophys. 105 (1982) 326–328.
[43] H. Yoshimura, Nonlinear astrophysical dynamos: Bifurcation of steady dynamos from oscillating dynamos, Astrophys. J. 221 (1978) 1088–1099.
[44] J.P. Cox, Pulsating stars, Rep. Prog. Phys. 37 (1974) 563–698.
[45] M. Barranco, J.R. Buchler and M. Livio, Thermal limit cycle oscillations on the surface of accreting neutron stars – X-ray bursters, Astrophys. J. 242 (1980) 1226–1231.
[46] J. Kuijpers and J.E. Pringle, Comments on radial white dwarf accretion, Astron. Astrophys. 114 (1982) L4–L6.
[47] A.G. Hearn, N.P.M. Kuin and P.C.H. Martens, Relaxation oscillations and double temperature structures in stellar coronae, Astron. Astrophys. 125 (1983) 69–74.
[48] A.G. Hearn and I.M. Vardavas, Models for stellar coronae: Numerical methods and examples, Astron. Astrophys. 98 (1981) 230–240.
[49] A.G. Hearn and I.M. Vardavas, Models for stellar coronae: Differences between hydrostatic and dynamic models, Astron. Astrophys. 98 (1981) 246–247.
[50] E.N. Parker, Dynamics of the interplanetary gas and magnetic fields, Astrophys. J. 128 (1958) 664–676.
[51] P. Souffrin, On the theory of shock-heated atmospheres: III. Discussion of the formalism and application to stellar coronae, Astron. Astrophys. 109 (1982) 205–212.
[52] G.B. Field, Thermal instability, Astrophys. J. 142 (1965) 531–567.
[53] N.P.M. Kuin and P.C.H. Martens, On the thermal stability of hot coronal loops: The coupling between chromosphere and corona, Astron. Astrophys. 108 (1982) L1–L4.
[54] J.E. Vernazza, E.H. Avrett and R. Loeser, Structure of the solar chromosphere: III. Models of the EUV brightness components of the quiet sun, Astrophys. J. Suppl. 45 (1981) 635–725.
[55] S.K. Antiochus, The stability of solar coronal loops, Astrophys. J. 232 (1979) L125–L129.
[56] A.W. Hood and E.R. Priest, Are solar coronal loops in thermal equilibrium?, Astron. Astrophys. 87 (1980) 126–131.
[57] C. Chiuderi, G. Einaudi and G. Torricelli-Ciamponi, What can we learn from static models of coronal loops?, Astron. Astrophys. 97 (1981) 27–32.
[58] P.V. Foukal, The pressure and energy balance of the cool corona over sunspots, Astrophys. J. 210 (1976) 575–581.
[59] J.P. Pye, K.D. Evans, R.J. Hutcheon, M. Gerassimenko, J.M. Davis, A.S. Krieger and J.F. Vesecky, The structure of the X-ray bright corona above active region McMath 12628 and derived implications for the description of equilibria in the solar atmosphere, Astron. Astrophys. 65 (1978) 123–138.
[60] H. Bénard, Les tourbillons cellulaires dans une nappe liquide transportant de la chaleur par convection en régime permanent, Ann. Chim. Phys. 23, Serie 7 (1901) 62–144.
[61] L.D. Landau, On the problem of turbulence, Comptes Rendus de l'Academie des Sciences de l'USSR, ns XLIV, 8 (1944) 311–314.
[62] E. Hopf, A mathematical example displaying features of turbulence, Commun. Pure Appl. Math. 1 (1948) 303–322.
[63] L.D. Landau and E.M. Lifshitz, Fluid Mechanics (Pergamon Press, Oxford, 1959).
[64] J.P. Gollub, S.V. Benson and J. Steinman, A subharmonic route to turbulent convection, in: Nonlinear Dynamics, The Annals of the New York Academy of Sciences, Vol. 357, ed. R.H.G. Helleman (The New York Academy of Sciences, New York, 1980) pp. 22–27.
[65] J. Bass, Les Fonctions Pseudo-Aléatoires, Mémorial des Sciences Mathématiques (Gauthiers Villars, Paris, 1962).

[66] D.D. Joseph, Stability of Fluid Motions I, Springer Tracts in Natural Philosophy, Vol. 27 (Springer, Berlin, 1976) chaps. 2 and 16.
[67] D. Ruelle and F. Takens, On the nature of turbulence, Commun. Math. Phys. 20 (1971) 167–192.
[68] R.M. May (ed.), Theoretical Ecology: Principles and Applications (Blackwell, Oxford, 1976).
[69] R.M. May, Simple mathematical models with very complicated dynamics, Nature 261 (1976) 459–467.
[70] D.R. Hofstadter, Strange attractors: Mathematical patterns delicately poised between order and chaos, Metamagical Themas, Scient. Am. 245 (5) (1981) 16–29.
[71] T.Y. Li and Y.A. Yorke, Period Three Implies Chaos, Am. Math. Monthly 82 (1975) 985–992.
[72] J. Guckenheimer, Endomorphisms of the Riemann Sphere, Proc. AMS Symposia in Pure Math. XIV (1970) 95–123.
[73] J.A. Yorke and E.D. Yorke, Chaotic behaviour and fluid dynamics, in: Hydrodynamic Instabilities and the Transition to Turbulence, Topics in Applied Physics, Vol. 45, eds. H.L. Swinney and J.P. Gollub (Springer, Berlin, 1981) pp. 77–94.
[74] M.J. Feigenbaum, Metric universality in nonlinear recurrence, in: Stochastic Behaviour in Classical and Quantum Hamiltonian Systems, Lecture Notes in Physics, Vol. 93, eds. G. Casati and J. Ford (Springer, Berlin, 1979) pp. 163–166.
[75] Program of the 1982 Dynamics Days Twente, Spring Conf. (Twente University of Technology, Enschede, The Netherlands, 1982).
[76] M.I. Rabinovich, Stochastic self-oscillations and turbulence, Sov. Phys. Usp. 21(5) (1978) 443–469.
[77] E.N. Lorenz, Deterministic nonperiodic flow, J. Atmos. Sci. 20 (1963) 130–141.
[78] B. Saltzman, Finite amplitude free convection as an initial value problem, I, J. Atmos. Sci. 19 (1962) 329–341.
[79] E.A. Spiegel and G. Veronis, On the Boussinesq approximation for a compressible fluid, Astrophys. J. 131 (1960) 442–447.
[80] J.B. McLaughlin and P.C. Martin, Transition to turbulence in a statistically stressed fluid system, Phys. Rev. A12 (1975) 186–203.
[81] C. Sparrow, The Lorenz Equations: Bifurcations, Chaos and Strange Attractors, Applied Mathematical Sciences Vol. 41 (Springer, Berlin, 1982).
[82] R.H.G. Helleman, Self-generated chaotic behaviour in non-linear mechanics, in: Fundamental Problems in Statistical Mechanics, Vol. 5, ed. E.G.D. Cohen (North-Holland, Amsterdam and New York, 1980) pp. 165–233.
[83] I. Bendixson, Sur les courbes définiés par des equations différentielles, Acta Math. 24 (1901) 1–88.
[84] O.E. Rössler, An equation for continuous chaos, Phys. Lett. 57A (1976) 397–398.
[85] D.R. Moore, J. Toomre, E. Knobloch and N.O. Weiss, Period doubling and chaos in partial differential equations, Nature 303 (1983) 663–667.
[86] E. Knobloch and N.O. Weiss, Bifurcations in a model of double-diffusive convection, Phys. Lett. 85A (1981) 127–130.
[87] M. Hénon and C. Heiles, The applicability of the third integral of motion: Some numerical experiments, Astron. J. 69 (1964) 73–79.
[88] M. Hénon, A two-dimensional mapping with a strange attractor, Commun. Math. Phys. 50 (1976) 69–77.
[89] M.L. Cartwright and J.E. Littlewood, On nonlinear differential equations of the second order: I. The equation $\ddot{y} + k(1 - y^2)\dot{y} + y = b\lambda k \cos(\lambda t + a)$, k large, J. London Math. Soc. 20 (1945) 180–189.
[90] J. Guckenheimer, Instabilities and chaos in nonhydrodynamic systems, in: Hydrodynamic Instabilities and the Transition to Turbulence, Topics in Applied Physics, Vol. 45, eds. H.L. Swinney and J.P. Gollub (Springer, Berlin, 1981) pp. 271–287.
[91] H. Poincaré, Les Méthodes Nouvelles de la Mécanique Céleste (Gauthiers-Villars, Paris, 1892; Dover Press, 1957).
[92] A. Einstein, Zum Quantensatz von Sommerfeld und Epstein, Verh. Deut. Phys. Ges. 19 (1917) 82–92.
[93] F.G. Gustavson, On constructing formal integrals of a Hamiltonian system near an equilibrium point, Astron. J. 71 (1966) 670–686.
[94] G. Contopoulos, Integrable and stochastic behaviour in dynamical astronomy, in: Proc. Volta Memorial Conf., eds. G. Casati and J. Ford (Springer Verlag, Berlin, 1979) pp. 1–17.
[95] Y.B. Zel'dovich and A.A. Ruzmaikin, Dynamo problems in astrophysics, in: Astrophysics and Space Physics Reviews, Section E of Soviet Scientific Reviews, Vol. 2, ed. R.A. Syunyaev (Harwood Academic Publishers, 1984) pp. 333–383.
[96] J.A. Eddy, The Maunder minimum, Science 192 (1976) 1189–1202.
[97] J.A. Eddy, The Maunder minimum: a reappraisal, Solar Phys. 89 (1983) 195–207.
[98] N.O. Weiss, Solar magnetism, in: Stellar and Planetary Magnetism, the Fluid Mechanics of Astrophysics and Geophysics, Vol. 2, ed. A.M. Soward (Gordon and Breach, 1983) pp. 115–131.
[100] T.G. Cowling, The magnetic field of sunspots, Mon. Not. R. Astron. Soc. 94 (1933) 39–48.
[101] E.N. Parker, Hydromagnetic dynamo models, Astrophys. J. 122 (1955) 293–314.
[102] E.N. Parker, Cosmic Magnetic Fields (Clarendon Press, Oxford, 1979).
[103] A. Pouquet, U. Frisch and J. Léorat, Strong MHD helical turbulence and the nonlinear dynamo effect, J. Fluid Mech. 77 (1976) 321–354.
[104] N.I. Kliorin and A.A. Ruzmaikin, Dynamics of the average turbulent helicity in a magnetic field, Magnetohydrodynamics 18 (1982) 116–122.
[105] F. Cattaneo, C.A. Jones and N.O. Weiss, Periodic and aperiodic behaviour in stellar dynamos, in: Solar and Stellar Magnetic Fields: Origins and Coronal Effects, I.A.U. Colloquium 102, ed. J.O. Stenflo (Reidel, Dordrecht, 1983) pp. 307–310.
[106] K.C. Tsinganos, J. Distler and R. Rosner, On the topological stability of magnetostatic equilibria, Astrophys. J. 278 (1984) 409–419.
[107] V.I. Arnold, Mathematical Methods of Classical Mechanics (Springer, Berlin, 1978).
[108] M.D. Kruskal and R.M. Kulsrud, Equilibrium of a magnetically confined plasma in a toroid, Phys. Fluids 1 (1958) 265–274.
[109] H. Goldstein, Classical Mechanics (sec. ed., Addison Wesley, 1980) §8.6.
[110] E.N. Parker, Topological dissipation and the small-scale fields in turbulent gases, Astrophys. J. 174 (1972) 499–510.
[111] H. Varvoglis and K. Papadopoulos, Selective nonresonant acceleration of $^3He^{++}$ and heavy ions by H^+ cyclotron waves, Astrophys. J. 270 (1983) L95–L98.
[112] H. Varvoglis, Chaotic ion motion in magnetosonic plasma waves, Astron. Astrophys. 132 (1984) 321–325.
[113] H.A. Lauwerier, Unpublished Lecture at the Dutch Astronomers Conf., Papendal 1982.

[114] M. Born, Continuity, Determinism and Reality, Ausgewählte Abhandlungen, Erster Band (Vandenhoeck & Ruprecht, Göttingen, 1963) pp. 196–219 (from: Dan. Mat. Fys. Medd. 30(2) (1955) 265).

[115] D. Ruelle, Les attracteurs etranges, La Recherche 11 (1980) 132–144.

[116] D. Farmer, J. Crutchfield, H. Froehling, N. Packard and R. Shaw, Power spectra and mixing properties of strange attractors, in: Nonlinear Dynamics, The Annals of the New York Academy of Sciences, Vol. 357, ed. R.H.G. Helleman (The New York Academy of Sciences, New York, 1980) pp. 453–472.

[117] F. Fárnik, J. Kaastra, B. Kálmán, M. Karlický, C. Slottje and B. Valníček, X-ray, Hα and Radio observations of the two-ribbon flare of May 16, 1981, Solar Phys. 89 (1983) 355–378.

[118] C.V. Solodyna, M. Gerassimenko and J.T. Nolte, Rapidly brightening X-ray coronal loops, American Science and Engineering Preprint 4303 (1978).